Generalized quasiharmonic approximation via space group irreducible derivatives

Mark A. Mathis, Amey Khanolkar, Lyuwen Fu, Matthew S. Bryan, Cody A. Dennett, Karl Rickert, J. Matthew Mann, Barry Winn, Douglas L. Abernathy, Michael E. Manley, David H. Hurley, and Chris A. Marianetti

The generalized quasiharmonic approximation via space group irreducible derivatives

Mark A. Mathis[1], Amey Khanolkar[2], Lyuwen Fu[1], Matthew S. Bryan[3], Cody A. Dennett[2], Karl Rickert[4], J. Matthew Mann[5], Barry Winn[6], Douglas L. Abernathy[6], Michael E. Manley[3], David H. Hurley[2], Chris A. Marianetti[1]

[1] *Department of Applied Physics and Applied Mathematics, Columbia University, New York, NY 10027*
[2] *Materials Science and Engineering Department,*
Idaho National Laboratory, Idaho Falls, ID 83415, USA
[3] *Materials Science and Technology Division, Oak Ridge National Laboratory, Oak Ridge, TN, 37831, USA*
[4] *KBR, 2601 Mission Point Boulevard, Suite 300, Dayton, OH 45431, USA*
[5] *Air Force Research Laboratory, Sensors Directorate,*
2241 Avionics Circle, Wright Patterson AFB, OH 45433, USA   and
[6] *Neutron Scattering Division, Oak Ridge National Laboratory, Oak Ridge, TN 37831, USA*

The quasiharmonic approximation (QHA) is the simplest nontrivial approximation for interacting phonons under constant pressure, bringing the effects of anharmonicity into temperature dependent observables. Nonetheless, the QHA is often implemented with additional approximations due to the complexity of computing phonons under arbitrary strains, and the generalized QHA, which employs constant stress boundary conditions, has not been completely developed. Here we formulate the generalized QHA, providing a practical algorithm for computing the strain state and other observables as a function of temperature and true stress. We circumvent the complexity of computing phonons under arbitrary strains by employing irreducible second order displacement derivatives of the Born-Oppenheimer potential and their strain dependence, which are efficiently and precisely computed using the lone irreducible derivative approach. We formulate two complementary strain parametrizations: a discretized strain grid interpolation and a Taylor series expansion in symmetrized strain. We illustrate our approach by evaluating the temperature and pressure dependence of select elastic constants and the thermal expansion in thoria (ThO_2) using density functional theory with three exchange-correlation functionals. The QHA results are compared to our measurements of the elastic constant tensor using time domain Brillouin scattering and inelastic neutron scattering. Our irreducible derivative approach simplifies the implementation of the generalized QHA, which will facilitate reproducible, data driven applications.

I. INTRODUCTION

Computing vibrational observables of insulating crystals requires the solution of an interacting phonon problem, which is highly nontrivial to solve in general. The simplest approach is to ignore all anharmonic terms in the Born-Oppenheimer potential, known as the harmonic approximation, whereby the partition function can be analytically written in terms of the phonon frequencies. However, the harmonic approximation does not capture many basic phenomena, such as thermal expansion, finite thermal conductivity, etc., and more sophisticated approximations are required. Perhaps the next simplest approach, specific to the case of constant pressure, is the well known quasiharmonic approximation (QHA) [1–6], whereby the anharmonicity is only accounted for via the strain dependence of the phonons and the elastic energy. The QHA is simple in that one still evaluates a quadratic partition function in the canonical ensemble, but the QHA partition function is explicitly a function of strain. The resulting Helmholtz free energy as a function of temperature and volume can then be Legendre transformed to the Gibbs free energy as a function of temperature and pressure, yielding observables that are measured under the usual experimental conditions. The QHA is a simple theory which gives a baseline description of the thermodynamics of an anharmonic crystal, and it is important to be able to implement the theory efficiently, accurately,

and with a minimal amount of information. Furthermore, it is important to be able to execute the QHA under the most general conditions of constant stress, as opposed to the case of constant pressure. To achieve these goals, we implement the generalized QHA purely using space group irreducible derivatives.

In practice, an infinite crystal is approximated by a finite crystal, whereby a homomorphism is constructed between the infinite translation group and a finite translation group; and the latter can be characterized by all translations within some supercell. The degrees of freedom of the finite crystal will be the lattice strains and the nuclear displacements, where the latter are defined relative to the minimum energy configuration at a given strain. The only inputs needed for the QHA are the Born-Oppenheimer potential for zero nuclear displacement as a function of strain (i.e., elastic energy) and the second nuclear displacement derivatives of the Born-Oppenheimer potential (i.e., the dynamical matrix) as a function of strain. Given that the numerically exact strain dependence of the elastic energy and the dynamical matrix can only be evaluated at discrete values of strain, some parametrization is needed in order to transform from the Helmholtz ensemble to the Gibbs ensemble. There are two natural strain parametrizations: a Taylor series as a function of strain truncated at a given order, or values on a discrete grid of strains which are then interpolated. Both parametrizations may be applied to the Helmholtz free energy or to its components (i.e., the elastic energy

and the dynamical matrices). Both the Taylor series and grid interpolations can be found in the literature, in addition to others, and we review some representative papers from this perspective. A key goal of our paper will be to implement both approaches from the perspective of space group irreducible derivatives.

We begin by reviewing papers based on the parametrization of the elastic energy. A very common approach is to fit the elastic energy to an equation of state [7–14]. While the equation of state approach is very popular, it has very clear disadvantages. Most importantly, the equation of state approach typically does not yield numerically exact descriptions of specific aspects of the elastic energy, unlike the Taylor series or the grid interpolation approach. The equation of state approach appears to be relevant only due to historical reasons, given that first-principles approaches were still computationally challenging at the level of a primitive unit cell many decades ago when equations of state were first applied in this context. Alternatively, several studies computed the elastic energy on a grid of strains and interpolated [15, 16]. The advantage of the grid interpolation approach is that the elastic energy is numerically exact at the grid points, though nothing is guaranteed between the grid points. So long as a sufficiently dense grid is precisely computed, the parametrization will faithfully describe the true function. A final approach would be to use a Taylor series expansion, which consists of both the linear and nonlinear elastic constants. The advantage of the Taylor series approach is that the elastic energy is numerically exact up to some order in strain, so long as the derivatives are faithfully computed. While nonlinear elastic constants have been computed from first-principles [17–21] and have been invoked in the early QHA literature [2, 22], we are not aware of their use in modern QHA calculations.

The computation of the dynamical matrix as a function of strain is far more computationally expensive than the computation of the elastic energy. Whether using a Taylor series or a grid-interpolation, it is important to address a common shortcoming in the literature. Some studies interpolate or expand purely in terms of the phonon frequencies, which can be problematic given that phonon modes cannot always be uniquely distinguished as a function of strain; though approaches have been developed to mitigate this problem [10, 13]. A robust approach is to parametrize the elements of the dynamical matrix as a function of strain, and preferably only the irreducible components, as executed in our approach. In terms of the grid interpolation approach, many studies evaluate the free energy on a grid of strains and interpolate [5, 11, 12, 15, 16], which involves splining a scalar function at each temperature as opposed to splining the dynamical matrix as a function of strain one time. In terms of Taylor series expanding in strain, the original idea of Gruneisen amounts to expanding the phonon frequencies to first order, encapsulated by the well known mode resolved Gruneisen parameters [1, 3, 23]. The Tay-

lor series in terms of phonon frequencies can naturally be extended to higher order for greater accuracy, and recent work has computed the frequencies up to second order in strain [13]. Our Taylor series approach expands the dynamical matrix instead of the phonon frequencies, and the latter can be exactly recovered as a subset of our result.

Another approach for parametrizing strain dependence would be to use a combination of a strain grid and Taylor series[24, 25]. In crystals where the point symmetry allows more than one degree of freedom in the lattice vectors (i.e. multiple identity strains), one must parametrize a multidimensional strain space, which can be computationally demanding. These situations naturally invite a combined strain grid and Taylor series approach. One begins by determining the lattice parameters as a function of volume by minimizing the Born-Oppenheimer potential at each volume on a grid, defining a one dimensional strain path through the multidimensional strain space. Subsequently, one can perform a Taylor series about each grid point along this one dimensional path, fully parametrizing the multidimensional strain space to some desired resolution. Solely constructing the one dimensional strain path already exactly recovers the classical zero temperature strain at arbitrary pressures, making it a useful approximation in general, and this approach has been explored in several studies [24, 26], and goes under the name of the statically-constrained QHA. Additionally, the leading order Taylor series about the one dimensional path has been explored [25].

Due to the complexity of fully implementing the generalized QHA (see Section III A for a precise definition), additional approximations have been introduced in the literature, such as the quasistatic approximation (QSA) [27]. The QSA evaluates the strain as a function of temperature using the QHA, but then computes the elastic constants at a given temperature by evaluating the relevant strain derivatives of the elastic energy at the strain prescribed by the QHA; as opposed to evaluating the strain derivatives of the free energy at that strain. The QSA removes the need for computing the phonons as a function of the strains that do not transform like the identity representation of the point group, greatly reducing the computational requirements for high symmetry crystals. The validity of the QSA has been shown to be insufficient in particular cases [16, 28], where QSA results are sometimes denoted as "cold curves", and therefore the QSA should be avoided if possible.

The material system being investigated in our study is thoria (ThO$_2$), an actinide-bearing crystal that has garnered interest as a next-generation nuclear fuel for power generation [29]. The ground state crystal structure of thoria is the flourite structure, which has space group $Fm\bar{3}m$ (225). A number of studies have used *ab initio* methods to predict finite temperature properties of thoria [30–36], however there is limited experimental data available for comparison. While there have been multiple studies on thermal expansion [37–40], there are only

two studies that measured the elastic constants of thoria at room temperature [41, 42].

In this paper, we present the generalized QHA, allowing for the evaluation of vibrational observables under conditions of constant temperature and true stress, while treating anharmonicity at the same level as the standard QHA. The generalized QHA is formulated purely in terms of space group irreducible derivatives, allowing the theory to be executed at a minimal computational cost. We execute the generalized QHA using density functional theory (DFT) with three different exchange-correlation functionals, yielding the temperature and pressure dependence of the elastic constant tensor and the thermal expansion. Various experimental measurements are also performed in our study. The thermal expansion is measured using a combination of X-ray diffraction and elastic neutron scattering; phonon frequencies are measured by inelastic neutron scattering at temperatures of 5 K, 300 K, and 750 K; time domain Brillouin scattering is used to measure the elastic constants at temperatures between 77 K and 350 K; and the temperature dependence of the shear strain elastic constant is measured by inelastic neutron scattering.

The rest of the paper is organized as follows. Section II formulates crystal vibrations at constant temperature under a general state of Biot strain or true stress. Section III presents the generalized quasiharmonic methodology, in addition to the implementation using space group irreducible derivatives. Section IV documents the experimental methods used, and Section V documents the details of the DFT calculations. Section VI presents our QHA and experimental results, and Section VII presents our conclusions.

II. GENERALIZED FORMALISM FOR CRYSTAL VIBRATIONS

A. Crystal vibrations under constant temperature and strain

We begin by considering a crystal, consisting of a periodic array of nuclei and a corresponding number of electrons. The Born-Oppenheimer (BO) potential is obtained by solving for the ground state energy of the many-electron Hamiltonian as a function of the nuclear positions. A phononic many-body problem is defined by the mass of the nuclei and the BO potential, and the resulting Hamiltonian may then be used to evaluate vibrational observables classically or quantum mechanically. The BO potential presumes that the electrons are at zero temperature, which will be a good approximation for insulators with electronic band gaps that far exceed $k_B T$. However, even when studying metals, the contribution from finite temperature electrons to lattice observables (e.g. thermal expansion) is often negligible [16, 43, 44]. Of course, there will be systems where the finite temperature electronic contributions will be important, such as

certain systems with charge density waves, and in such cases a theory beyond the Born-Oppenheimer approximation must be employed. A more general approach replaces the BO potential with an effective potential obtained by solving the electronic many-body problem at a finite electronic temperature as a function of the nuclear positions [45–48]. Such a potential can be immediately incorporated within our theoretical framework and the generalized QHA (see Section III), though here we restrict our discussion to the more usual case of the BO potential for simplicity.

The crystal structure is defined by three primitive lattice vectors, which we store as a row stacked 3×3 matrix $\hat{\mathbf{a}}$, and basis atom positions defined by vectors $\mathbf{A}_i$, where $i = 1, \ldots, n_a$ and n_a is the number of atoms in the primitive unit cell. The reciprocal lattice vectors are then defined as a row stacked matrix $\hat{\mathbf{b}} = 2\pi(\hat{\mathbf{a}}^{-1})^{\mathsf{T}}$. The crystal structure will be invariant to some space group, which will yield one or more variable degrees of freedom when defining $\hat{\mathbf{a}}$ and $\mathbf{A}_i$. The degrees of freedom within $\hat{\mathbf{a}}$ and $\mathbf{A}_i$ are then determined by minimizing over the BO potential, and the result is the classical lattice parameters and classical basis atom positions at zero temperature and stress, denoted by $\hat{\mathbf{a}}_o$ and $\mathbf{A}_{o,i}$, respectively.

The strained lattice vectors are encoded by the function $\hat{\mathbf{a}}(\boldsymbol{\epsilon})$, where $\boldsymbol{\epsilon}$ is a vector of the six independent strain amplitudes (see Section II B). The classical basis atom positions will be functions of strain $\mathbf{A}_i(\boldsymbol{\epsilon})$, and the positions are determined by minimizing the BO potential with respect to the degrees of freedom within the space group of the strained lattice (see Appendix B for a mathematical definition). For strains that transform like the identity representation of the point group (i.e., identity strains), the space group will be unchanged, while for non-identity strains the space group will be lowered and there may be additional degrees of freedom within the basis atoms $\mathbf{A}_i(\boldsymbol{\epsilon})$. The atomic displacements $u_{\mathbf{q}}^{(j)}$ are defined relative to the nuclear positions generated by $\hat{\mathbf{a}}(\boldsymbol{\epsilon})$ and $\mathbf{A}_i(\boldsymbol{\epsilon})$, where $\mathbf{q} \in \mathbb{R}^3$ is the lattice coordinate of a Cartesian reciprocal lattice point $\mathbf{Q}(\boldsymbol{\epsilon}) = \mathbf{q}\hat{\mathbf{b}}(\boldsymbol{\epsilon})$ within the first Brillouin zone, and j labels either a two tuple of an atom in the primitive unit cell and its displacement vector or an irreducible representation of the little group of $\mathbf{q}$ and an integer labeling the instance if the irreducible representation is repeated. It should be emphasized that $\mathbf{A}_i(\boldsymbol{\epsilon})$ are reference points from which $u_{\mathbf{q}}^{(j)}$ are defined, and should not be confused with the expectation value of $\mathbf{q} = \mathbf{0}$ displacements, which determine the average crystal structure at finite temperature and strain $\boldsymbol{\epsilon}$ (see Appendix B for further discussion).

We now define a function $\mathcal{V}(\boldsymbol{\epsilon}, \mathbf{u})$ which yields the BO potential energy, and the independent variables are $\boldsymbol{\epsilon}$ and $\mathbf{u}$, where $\mathbf{u}$ is a vector of all displacements $\{u_{\mathbf{q}}^{(j)}\}$. The nuclei are now treated quantum mechanically, with the potential energy being $\mathcal{V}(\boldsymbol{\epsilon}, \mathbf{u})$. The generalized Helmholtz free energy $F(T, \boldsymbol{\epsilon})$ of the crystal can now be formally constructed by exactly evaluating the quantum partition

function.

B. Strain measures and representations

The strain measure parameterizes the non-rotational component of the deformation of the lattice vectors, and there are an infinite number of strain measures [49, 50]. The Lagrangian strain measure is commonly used in the context of nonlinear elastic constants [17–21], and it is appealing given that the conjugate stress (i.e. the second Piola-Kirchhoff stress) is inherently symmetric and it is straightforward to change the reference lattice. However, the Lagrangian strain is less convenient when parametrizing the dynamical matrix and the elastic energy as a function of strain, and instead it is preferable to use the Biot strain, which is straightforward to symmetrize and generates a linear change in the lattice vectors. The chain rule can be used to convert from Biot strain derivatives to Lagrangian strain derivatives when desired. Therefore, we use Biot strain to parametrize the strain dependence of $\mathcal{V}(\boldsymbol{\epsilon}, \mathbf{u})$ and use Lagrangian strain when changing the reference lattice.

A general transformation of the lattice vectors $\hat{\mathbf{a}}_o$ to a new set of lattice vectors $\hat{\mathbf{a}}$ is given by

$$\hat{\mathbf{a}} = \hat{\mathbf{a}}_o \hat{\mathbf{F}}^{\mathsf{T}}, \tag{1}$$

where $\hat{\mathbf{F}}$ is an invertible matrix referred to as the deformation matrix. In general, $\hat{\mathbf{F}}$ may describe stretches and rotations of the lattice, as evidenced by the polar decomposition theorem

$$\hat{\mathbf{F}} = \hat{\mathbf{V}}\hat{\mathbf{R}} = \hat{\mathbf{R}}\hat{\mathbf{U}}, \tag{2}$$

where $\hat{\mathbf{V}}$ and $\hat{\mathbf{U}}$ are unique, positive definite, symmetric matrices referred to as the left and right stretch matrix, respectively, and $\hat{\mathbf{R}}$ is a unique orthogonal matrix referred to as the rotation matrix. Given that the rotation does not deform the lattice, it is desirable to only parametrize some function of the stretch matrices. One possibility is the right stretch matrix itself, which can be recast as $\hat{\mathbf{U}} = \hat{\mathbf{1}} + \hat{\boldsymbol{\epsilon}}$, where

$$\hat{\boldsymbol{\epsilon}} \equiv \begin{bmatrix} \epsilon_1 & \frac{1}{2}\epsilon_6 & \frac{1}{2}\epsilon_5 \\ \frac{1}{2}\epsilon_6 & \epsilon_2 & \frac{1}{2}\epsilon_4 \\ \frac{1}{2}\epsilon_5 & \frac{1}{2}\epsilon_4 & \epsilon_3 \end{bmatrix}, \tag{3}$$

which is referred to as the Biot strain [49]. As mentioned previously, another common choice of strain measure is the Lagrangian strain, defined as

$$\hat{\boldsymbol{\eta}} = \frac{1}{2}(\hat{\mathbf{F}}^{\mathsf{T}}\hat{\mathbf{F}} - \hat{\mathbf{1}}) = \frac{1}{2}(\hat{\mathbf{U}}^2 - \hat{\mathbf{1}}) = \hat{\boldsymbol{\epsilon}} + \frac{1}{2}\hat{\boldsymbol{\epsilon}}^2. \tag{4}$$

We utilize the Lagrangian strain as an intermediate step in the process of constructing true stress and elastic constants at finite strains.

It is natural to encode a symmetric matrix in terms of the independent components, which is relevant given that $\hat{\boldsymbol{\epsilon}}$, $\hat{\boldsymbol{\eta}}$, and the true stress are all symmetric. For example, the state of strain $\hat{\boldsymbol{\epsilon}}$ in terms of the six independent components can be encoded by a vector

$$\boldsymbol{\epsilon} = [\epsilon_1, \epsilon_2, \epsilon_3, \epsilon_4, \epsilon_5, \epsilon_6]^{\mathsf{T}}, \tag{5}$$

where the ordering is consistent with Voigt notation. Each strain amplitude ϵ_i can be obtained by projecting the Biot strain $\hat{\boldsymbol{\epsilon}}$ along the corresponding basis vector $\hat{\boldsymbol{\lambda}}_i$ as

$$\epsilon_i = \frac{\operatorname{tr}\left(\hat{\boldsymbol{\epsilon}}\hat{\boldsymbol{\lambda}}_i\right)}{\operatorname{tr}\left(\hat{\boldsymbol{\lambda}}_i\hat{\boldsymbol{\lambda}}_i\right)}, \tag{6}$$

where $\hat{\boldsymbol{\lambda}}_i$ is a real 3×3 matrix which is a linear combination of the Gell-Mann matrices (see Ref. [51], Section SIV for definitions). The Biot strain can be then written in terms of its components as $\hat{\boldsymbol{\epsilon}} = \sum_i \epsilon_i \hat{\boldsymbol{\lambda}}_i$. A corresponding vector $\boldsymbol{\eta}$ will be used for the Lagrangian strain.

Strain can by symmetrized according to the irreducible representations of the point group of the space group using standard group theoretical techniques, which is necessary for constructing relevant selection rules. For the case of the O_h point group, symmetrization of strain yields $A_{1g} \oplus E_g \oplus T_{2g}$, and the resulting symmetrized basis vectors are

$$\hat{\boldsymbol{\lambda}}_{A_{1g}} = \frac{1}{\sqrt{3}}(\hat{\boldsymbol{\lambda}}_1 + \hat{\boldsymbol{\lambda}}_2 + \hat{\boldsymbol{\lambda}}_3), \tag{7}$$

$$\hat{\boldsymbol{\lambda}}_{E_g^0} = \frac{1}{\sqrt{2}}(\hat{\boldsymbol{\lambda}}_1 - \hat{\boldsymbol{\lambda}}_2), \tag{8}$$

$$\hat{\boldsymbol{\lambda}}_{E_g^1} = \frac{1}{\sqrt{6}}(2\hat{\boldsymbol{\lambda}}_3 - \hat{\boldsymbol{\lambda}}_1 - \hat{\boldsymbol{\lambda}}_2), \tag{9}$$

$$\hat{\boldsymbol{\lambda}}_{T_{2g}^0} = \hat{\boldsymbol{\lambda}}_6, \quad \hat{\boldsymbol{\lambda}}_{T_{2g}^1} = \hat{\boldsymbol{\lambda}}_4, \quad \hat{\boldsymbol{\lambda}}_{T_{2g}^2} = \hat{\boldsymbol{\lambda}}_5, \tag{10}$$

where the superscript on the irreducible representation label indicates a given row of a multidimensional irreducible representation.

Given that the energy is invariant to a rotation of the lattice, only symmetric deformations of the lattice must be considered during parameterization. Therefore, we define the symmetrically deformed lattice as a function of the Biot strain as

$$\hat{\mathbf{a}}(\boldsymbol{\epsilon}) = \hat{\mathbf{a}}_o(\hat{\mathbf{1}} + \hat{\boldsymbol{\epsilon}}), \quad \hat{\mathbf{R}} = \hat{\mathbf{1}}. \tag{11}$$

The key task is then to parameterize the dynamical matrix and the elastic energy as a function of $\boldsymbol{\epsilon}$. In order to construct Lagrangian strain derivatives from Biot strain derivatives, the following partial derivatives are needed

$$\frac{\partial \eta_i}{\partial \epsilon_j} = \delta_{ij} + \frac{1}{2} \operatorname{tr}\left(\hat{\boldsymbol{\lambda}}_i^2\right)^{-1} \sum_k \epsilon_k \operatorname{tr}\left(\hat{\boldsymbol{\lambda}}_i(\hat{\boldsymbol{\lambda}}_k\hat{\boldsymbol{\lambda}}_j + \hat{\boldsymbol{\lambda}}_j\hat{\boldsymbol{\lambda}}_k)\right), \tag{12}$$

$$\frac{\partial^2 \eta_i}{\partial \epsilon_j \partial \epsilon_k} = \frac{1}{2} \operatorname{tr}\left(\hat{\boldsymbol{\lambda}}_i^2\right)^{-1} \operatorname{tr}\left(\hat{\boldsymbol{\lambda}}_i(\hat{\boldsymbol{\lambda}}_k\hat{\boldsymbol{\lambda}}_j + \hat{\boldsymbol{\lambda}}_j\hat{\boldsymbol{\lambda}}_k)\right). \tag{13}$$

In the case of a cubic crystal where there are only finite A_{1g} strains with amplitude $\epsilon_{A_{1g}}$, Eq. 12 simplifies to

$$\frac{\partial \eta_i}{\partial \epsilon_j} = \delta_{ij}(1 + \frac{\sqrt{3}}{3}\epsilon_{A_{1g}}), \quad O_h \text{ Point Group.} \quad (14)$$

1. Change in reference lattice

In the preceding, the deformation matrix and corresponding strain are defined with respect to a single reference lattice $\hat{\mathbf{a}}_o$. However, it is necessary to change from one reference lattice to another when constructing the true stress and true elastic constants, and it is most convenient to work with the Lagrangian strain. We proceed by defining deformations relative to two lattices, $\hat{\mathbf{a}}_1$ and $\hat{\mathbf{a}}_2$, as parameterized by the Lagrangian strain $\boldsymbol{\eta}_1$ and $\boldsymbol{\eta}_2$, respectively. The Lagrangian strain $\boldsymbol{\eta}_1$ in terms of $\hat{\mathbf{a}}$ is written using equations 1 and 4,

$$\hat{\boldsymbol{\eta}}_1(\hat{\mathbf{a}}) = \frac{1}{2}(\hat{\mathbf{a}}_1^{-1}\hat{\mathbf{a}}(\hat{\mathbf{a}}_1^{-1}\hat{\mathbf{a}})^{\mathsf{T}} - \hat{\mathbf{1}}), \quad (15)$$

and the deformed lattice $\hat{\mathbf{a}}$ as a function of the Lagrangian strain $\boldsymbol{\eta}_2$ and the rotation $\hat{\mathbf{R}}$ is given by

$$\hat{\mathbf{a}}(\boldsymbol{\eta}_2, \hat{\mathbf{R}}) = \hat{\mathbf{a}}_2\sqrt{2\hat{\boldsymbol{\eta}}_2 + \hat{\mathbf{1}}}\hat{\mathbf{R}}^{\mathsf{T}}, \quad (16)$$

The relation between the two strains is achieved using function composition,

$$\hat{\boldsymbol{\eta}}_1(\hat{\mathbf{a}}(\boldsymbol{\eta}_2, \hat{\mathbf{R}})) = \frac{1}{2}(\hat{\mathbf{a}}_1^{-1}\hat{\mathbf{a}}_2(2\hat{\boldsymbol{\eta}}_2 + \hat{\mathbf{1}})(\hat{\mathbf{a}}_1^{-1}\hat{\mathbf{a}}_2)^{\mathsf{T}} - \hat{\mathbf{1}}). \quad (17)$$

which is independent of the rotation $\hat{\mathbf{R}}$. Eq. 17 can then be used to construct partial derivatives from one strain measure to another as

$$\frac{\partial \eta_{1,i}}{\partial \eta_{2,j}} = \text{tr}\left(\hat{\boldsymbol{\lambda}}_i^2\right)^{-1}\text{tr}\left(\hat{\boldsymbol{\lambda}}_i\hat{\mathbf{a}}_1^{-1}\hat{\mathbf{a}}_2\hat{\boldsymbol{\lambda}}_j(\hat{\mathbf{a}}_1^{-1}\hat{\mathbf{a}}_2)^{\mathsf{T}}\right). \quad (18)$$

In order to construct the true stress at a lattice $\hat{\mathbf{a}}(\boldsymbol{\epsilon})$, the reference lattice must be changed from $\hat{\mathbf{a}}_o$ to the current lattice $\hat{\mathbf{a}}(\boldsymbol{\epsilon})$. The Lagrangian strain constructed from the reference lattice $\hat{\mathbf{a}}(\boldsymbol{\epsilon})$ is denoted as $\underline{\boldsymbol{\eta}}$ (opposite to the naming convention of Wallace[52]). Taking $\boldsymbol{\eta}_1 = \boldsymbol{\eta}$, $\boldsymbol{\eta}_2 = \underline{\boldsymbol{\eta}}$, $\hat{\mathbf{a}}_1 = \hat{\mathbf{a}}_o$, and $\hat{\mathbf{a}}_2 = \hat{\mathbf{a}}(\boldsymbol{\epsilon})$, and substituting into Eq. 18 results in

$$\frac{\partial \eta_i}{\partial \underline{\eta}_j} = \text{tr}\left(\hat{\boldsymbol{\lambda}}_i^2\right)^{-1}\text{tr}\left(\hat{\boldsymbol{\lambda}}_i(\hat{\mathbf{1}} + \hat{\boldsymbol{\epsilon}})\hat{\boldsymbol{\lambda}}_j(\hat{\mathbf{1}} + \hat{\boldsymbol{\epsilon}})\right), \quad \hat{\mathbf{R}} = \hat{\mathbf{1}}, \quad (19)$$

which will be used in Eq. 24 when constructing the true stress. In the case of a cubic crystal, Eq. 19 simplifies to

$$\frac{\partial \eta_i}{\partial \underline{\eta}_j} = \delta_{ij}(1 + \frac{\sqrt{3}}{3}\epsilon_{A_{1g}})^2, \quad O_h \text{ Point Group.} \quad (20)$$

C. Crystal vibrations under constant temperature and true stress

Section II A introduced the many-phonon problem under conditions of constant strain. However, experiment is normally conducted under conditions of constant stress. Therefore, we need a formalism that can construct observables at some prescribed stress. For the simpler case of constant pressure, it is natural to Legendre transform the usual Helmholtz free energy to the Gibbs free energy. Generalizing the Legendre transform to the case of a general state of true stress is cumbersome given that it requires the use of true strain[49, 50]. Therefore, we invert the true stress equation in order to obtain the Biot strain as a function of temperature and true stress, allowing for the study of a given phase.

We begin by formulating the true stress as a function of temperature and strain $\boldsymbol{\epsilon}$ [49, 53] as

$$\hat{\boldsymbol{\sigma}}(T, \boldsymbol{\epsilon}, \hat{\mathbf{R}}) = \frac{|\hat{\mathbf{a}}_o|}{|\hat{\mathbf{a}}(\boldsymbol{\epsilon})|}\hat{\mathbf{F}}^{\mathsf{T}}\hat{\boldsymbol{\Sigma}}(T, \boldsymbol{\epsilon})\hat{\mathbf{F}}, \quad (21)$$

where $\hat{\mathbf{F}} = \hat{\mathbf{R}}(\hat{\mathbf{1}} + \hat{\boldsymbol{\epsilon}})$ and the i-th component of the Second Piola-Kirchhoff stress is

$$\Sigma_i(T, \boldsymbol{\epsilon}) = \frac{1}{|\hat{\mathbf{a}}_o|}\sum_j \frac{\partial F(T, \boldsymbol{\epsilon})}{\partial \epsilon_j}\bigg|_{\boldsymbol{\epsilon}} \frac{\partial \epsilon_j}{\partial \eta_i}\bigg|_{\boldsymbol{\epsilon}}, \quad (22)$$

Hereafter we specialize to the case of $\hat{\mathbf{R}} = \hat{\mathbf{1}}$, given that the orientation of the crystal will normally be fixed. Equation 21 can be projected onto the i-th component, or the chain rule can be used to generate the equivalent expression, yielding

$$\tilde{\sigma}_i(T, \boldsymbol{\epsilon}) = \text{tr}\left(\hat{\boldsymbol{\lambda}}_i\hat{\boldsymbol{\sigma}}(T, \boldsymbol{\epsilon}, \hat{\mathbf{1}})\right) \quad (23)$$

$$= \frac{1}{|\hat{\mathbf{a}}(\boldsymbol{\epsilon})|}\sum_{jk} \frac{\partial F(T, \boldsymbol{\epsilon})}{\partial \epsilon_j}\bigg|_{\boldsymbol{\epsilon}} \frac{\partial \epsilon_j}{\partial \eta_k}\bigg|_{\boldsymbol{\epsilon}} \frac{\partial \eta_k}{\partial \underline{\eta}_i}\bigg|_{\boldsymbol{\epsilon}}. \quad (24)$$

Having constructed the true stress as a function of temperature and $\boldsymbol{\epsilon}$, a strain map can be formally constructed via the inverse of Eq. 24 as

$$\tilde{\boldsymbol{\epsilon}}(T, \boldsymbol{\sigma}), \quad \text{where} \quad \tilde{\boldsymbol{\sigma}}(T, \tilde{\boldsymbol{\epsilon}}(T, \boldsymbol{\sigma})) = \boldsymbol{\sigma}. \quad (25)$$

The lattice vectors $\hat{\mathbf{a}}(T, \boldsymbol{\sigma})$ at a given temperature and true stress are then given by

$$\hat{\mathbf{a}}(T, \boldsymbol{\sigma}) = \hat{\mathbf{a}}_o(\hat{\mathbf{1}} + \sum_i \hat{\boldsymbol{\lambda}}_i\tilde{\epsilon}_i(T, \boldsymbol{\sigma})). \quad (26)$$

Given the importance of $\tilde{\boldsymbol{\epsilon}}(T, \boldsymbol{\sigma})$, it is useful to define the thermal strain tensor, analogous to the definition of Wallace [23], as

$$\alpha_i(T, \boldsymbol{\sigma}) \equiv \frac{\partial \tilde{\epsilon}_i(T, \boldsymbol{\sigma})}{\partial T}, \quad (27)$$

which can be rewritten via the chain rule as

$$\alpha_i(T, \boldsymbol{\sigma}) = -\sum_j \frac{\partial \tilde{\epsilon}_i(T, \boldsymbol{\sigma})}{\partial \sigma_j}\bigg|_{\boldsymbol{\sigma}} \frac{\partial \tilde{\sigma}_j(T, \boldsymbol{\epsilon})}{\partial T}\bigg|_{\tilde{\boldsymbol{\epsilon}}(T, \boldsymbol{\sigma})}. \quad (28)$$

1. Results for cubic crystals

For the case of cubic crystals under constant pressure, the only nonzero stress and strain components will be A_{1g}, and Eq. 24 can be simplified using equations 14 and 20, resulting in

$$\tilde{\sigma}_{A_{1g}}(T, \boldsymbol{\epsilon}(\epsilon_{A_{1g}})) = \frac{1}{|\hat{\mathbf{a}}_o|(1 + \frac{1}{\sqrt{3}}\epsilon_{A_{1g}})^2} \left. \frac{\partial F(T, \boldsymbol{\epsilon})}{\partial \epsilon_{A_{1g}}} \right|_{\boldsymbol{\epsilon}(\epsilon_{A_{1g}})}. \tag{29}$$

The strain map $\tilde{\boldsymbol{\epsilon}}(T, \boldsymbol{\sigma}(\sigma_{A_{1g}}))$ can be obtained to leading order in $\sigma_{A_{1g}}$ at an arbitrary temperature by evaluating the strain derivative of Eq. 29 at $\tilde{\epsilon}_{A_{1g}}(T, \mathbf{0})$ and inverting, which gives

$$\tilde{\epsilon}_{A_{1g}}(T, \boldsymbol{\sigma}(\sigma_{A_{1g}})) = \tilde{\epsilon}_{A_{1g}}(T, \mathbf{0}) +$$
$$\sigma_{A_{1g}} \frac{|\hat{\mathbf{a}}_o|(1 + \frac{1}{\sqrt{3}}\tilde{\epsilon}_{A_{1g}}(T, \mathbf{0}))^2}{\mathcal{C}_{A_{1g}A_{1g}}(T, \mathbf{0})} + \dots, \tag{30}$$

where $\mathcal{C}_{ij}(T, \boldsymbol{\sigma})$ is defined in Eq. 45. The A_{1g} element of the thermal strain tensor, defined in Eq. 27, can be explicitly evaluated as

$$\alpha_{A_{1g}}(T, \boldsymbol{\sigma}(\sigma_{A_{1g}})) = - \left. \frac{\partial^2 F(T, \boldsymbol{\epsilon})}{\partial \epsilon_{A_{1g}} \partial T} \right|_{\tilde{\boldsymbol{\epsilon}}(T, \boldsymbol{\sigma}(\sigma_{A_{1g}}))} \times$$
$$\left(\mathcal{C}_{A_{1g}A_{1g}}(T, \boldsymbol{\sigma}(\sigma_{A_{1g}})) - \frac{2\sigma_{A_{1g}}}{\sqrt{3}} \left(1 + \frac{\tilde{\epsilon}_{A_{1g}}(T, \boldsymbol{\sigma}(\sigma_{A_{1g}}))}{\sqrt{3}}\right) \right)^{-1}. \tag{31}$$

Given that various observables are encoded as a function of pressure or volume in a cubic crystal, it is useful to convert to these variables. The A_{1g} strain can be written as a function of the volumetric strain as

$$\epsilon_{A_{1g}}(\epsilon_v) = \sqrt{3}((1 + \epsilon_v)^{\frac{1}{3}} - 1), \tag{32}$$

and the volumetric strain can be written as a function of the volume as

$$\epsilon_v(V) = \frac{V - V_o}{V_o}, \tag{33}$$

where $V_o = |\hat{\mathbf{a}}_o|$. The nonzero components of stress under constant pressure in the standard and symmetrized basis, respectively, are given as

$$\sigma_1(P) = \sigma_2(P) = \sigma_3(P) = -P, \quad \sigma_{A_{1g}}(P) = -\sqrt{3}P. \tag{34}$$

Using equations 32 and 33, the usual coefficient of volumetric thermal expansion as a function of temperature and pressure can be constructed as

$$\alpha_v(T, P) = \frac{1}{V(T, P)} \frac{\partial V(T, P)}{\partial T} = \frac{3\alpha_{A_{1g}}(T, \boldsymbol{\sigma}(P))}{\sqrt{3} + \tilde{\epsilon}_{A_{1g}}(T, \boldsymbol{\sigma}(P))}, \tag{35}$$

and the coefficient of linear thermal expansion (CLTE) is given by

$$\alpha_l(T, P) = \frac{1}{a(T, P)} \frac{\partial a(T, P)}{\partial T} = \frac{\alpha_{A_{1g}}(T, \boldsymbol{\sigma}(P))}{\sqrt{3} + \tilde{\epsilon}_{A_{1g}}(T, \boldsymbol{\sigma}(P))}, \tag{36}$$

where $a(T, P)$ is the cubic lattice parameter as a function of temperature and pressure.

The preceding equations are all exact relations, and here we introduce the small strain approximation (SSA), which can be useful for constructing approximate equations which circumvent a numerical inversion of the strain map, Eq. 25. The essence of the SSA was introduced in the original work of Gruneisen[1], and this idea can be used to approximate arbitrary observables in terms of the exact free energy. The leading order SSA expression for $\tilde{\epsilon}_{A_{1g}}$ can be obtained by Taylor series expanding Eq. 29 to leading order in $\epsilon_{A_{1g}}$ about zero and inverting, yielding

$$\tilde{\epsilon}_{A_{1g}}^{(1)}(T, \boldsymbol{\sigma}(\sigma_{A_{1g}})) = \frac{|\hat{\mathbf{a}}_o|\sigma_{A_{1g}} - \dot{F}(T)}{\ddot{F}(T) - \frac{2}{\sqrt{3}}\dot{F}(T)} \tag{37}$$

where the superscript 1 denotes that the stress is expanded to first order in strain, and

$$\dot{F}(T) \equiv \left. \frac{\partial F(T, \boldsymbol{\epsilon})}{\partial \epsilon_{A_{1g}}} \right|_{\boldsymbol{\epsilon} = \mathbf{0}}, \quad \ddot{F}(T) \equiv \left. \frac{\partial^2 F(T, \boldsymbol{\epsilon})}{\partial \epsilon_{A_{1g}}^2} \right|_{\boldsymbol{\epsilon} = \mathbf{0}}. \tag{38}$$

Evaluating Eq. 37 within the generalized QHA recovers the usual Gruneisen relation (see Section III A 1).

D. Elastic constants at constant temperature and true stress

There are two types of experimentally relevant elastic constants under isothermal or adiabatic conditions [23, 52, 54]: $B_{\alpha\beta\gamma\delta}(T, \boldsymbol{\sigma})$ is the leading order expansion coefficient of the true stress with respect to strain and $S_{\alpha\beta\gamma\delta}(T, \boldsymbol{\sigma})$ is the coefficient which determines the dynamics of elastic wave propagation; where Greek subscripts label Cartesian indices (i.e. x, y, z). Both $B_{\alpha\beta\gamma\delta}(T, \boldsymbol{\sigma})$ and $S_{\alpha\beta\gamma\delta}(T, \boldsymbol{\sigma})$ depend on $C_{\alpha\beta\gamma\delta}(T, \boldsymbol{\sigma})$, which is the curvature of the Helmholtz free energy with respect to $\boldsymbol{\eta}$, where $\boldsymbol{\eta}$ is defined relative to $\hat{\mathbf{a}}(T, \boldsymbol{\sigma})$, divided by the current volume $|\hat{\mathbf{a}}(T, \boldsymbol{\sigma})|$. Given that $C_{\alpha\beta\gamma\delta}(T, \boldsymbol{\sigma})$ has full Voigt symmetry, we can construct

$$C_{ij}(T, \boldsymbol{\sigma}) \equiv C_{\alpha\beta\gamma\delta}(T, \boldsymbol{\sigma}), \tag{39}$$

where $i = v(\alpha, \beta)$ and $j = v(\gamma, \delta)$, and $v(\alpha, \beta)$ is the function which maps two Cartesian indices to the corresponding Voigt notation index. The coefficients $B_{\alpha\beta\gamma\delta}$ can be obtained as (see Ref. [52], Eq. 2.36)

$$B_{\alpha\beta\gamma\delta}(T, \boldsymbol{\sigma}) = C_{\alpha\beta\gamma\delta}(T, \boldsymbol{\sigma}) + \frac{1}{2}(\sigma_{v(\alpha,\gamma)}\delta_{\beta\delta} + \sigma_{v(\alpha,\delta)}\delta_{\beta\gamma}$$
$$+ \sigma_{v(\beta,\gamma)}\delta_{\alpha\delta} + \sigma_{v(\beta,\delta)}\delta_{\alpha\gamma} - 2\sigma_{v(\alpha,\beta)}\delta_{\gamma\delta}). \tag{40}$$

Similarly, the coefficients $S_{\alpha\beta\gamma\delta}$ can be obtained as (see Ref. [52], Eq. 2.24)

$$S_{\alpha\beta\gamma\delta}(T,\boldsymbol{\sigma}) = C_{\alpha\beta\gamma\delta}(T,\boldsymbol{\sigma}) + \delta_{\alpha\gamma}\sigma_{v(\beta,\delta)}. \qquad (41)$$

Elastic wave propagation is then determined by the acoustic matrix (similar to the case in Ref. [23]), defined as

$$A_{\mathbf{Q}}^{\alpha\beta}(T,\boldsymbol{\sigma}) = \frac{|\hat{\mathbf{a}}(T,\boldsymbol{\sigma})|}{|\mathbf{Q}|^2} \sum_{\gamma\delta} Q_\gamma Q_\delta S_{\gamma\alpha\delta\beta}(T,\boldsymbol{\sigma}), \qquad (42)$$

where $\mathbf{Q}$ is a Cartesian reciprocal lattice point. The velocities of elastic wave propagation are determined by finding the eigenvalues of the acoustic matrix

$$m v_{\mathbf{Q}}^i(T,\boldsymbol{\sigma})^2 \left|\psi_{\mathbf{Q}}^i(T,\boldsymbol{\sigma})\right\rangle = \hat{\mathbf{A}}_{\mathbf{Q}}(T,\boldsymbol{\sigma}) \left|\psi_{\mathbf{Q}}^i(T,\boldsymbol{\sigma})\right\rangle, \quad (43)$$

where m is the total mass in the primitive unit cell, $v_{\mathbf{Q}}^i$ is the velocity, and i is the band index which can be categorized according to irreducible representations of the little group of $\mathbf{Q}$.

The only nontrivial task is to compute $C_{ij}(T,\boldsymbol{\sigma})$, and then $C_{\alpha\beta\gamma\delta}(T,\boldsymbol{\sigma})$, $B_{\alpha\beta\gamma\delta}(T,\boldsymbol{\sigma})$, and $S_{\alpha\beta\gamma\delta}(T,\boldsymbol{\sigma})$ are immediately known. In the preceding discussion, all equations apply equally to isothermal and adiabatic conditions, and we now construct $C_{ij}(T,\boldsymbol{\sigma})$ in both cases. Beginning with $C_{ij}^{\mathrm{iso}}(T,\boldsymbol{\sigma})$, the chain rule is used to obtain

$$C_{ij}^{\mathrm{iso}}(T,\boldsymbol{\sigma}) = \frac{1}{|\hat{\mathbf{a}}(T,\boldsymbol{\sigma})|} \sum_{mn} \left(\sum_{kl} \mathcal{C}_{kl}(T,\boldsymbol{\sigma}) \frac{\partial\epsilon_k}{\partial\eta_m} \frac{\partial\epsilon_l}{\partial\eta_n} + \sum_k s_k(T,\boldsymbol{\sigma}) \frac{\partial^2\epsilon_k}{\partial\eta_m\partial\eta_n} \right) \frac{\partial\eta_m}{\partial\underline{\eta}_i} \frac{\partial\eta_n}{\partial\underline{\eta}_j}, \qquad (44)$$

where the partial derivatives may be obtained from Eq. 12 and Eq. 18, and

$$\mathcal{C}_{ij}(T,\boldsymbol{\sigma}) \equiv \left.\frac{\partial^2 F(T,\boldsymbol{\epsilon})}{\partial\epsilon_i\partial\epsilon_j}\right|_{\tilde{\boldsymbol{\epsilon}}(T,\boldsymbol{\sigma})}, \qquad (45)$$

and

$$s_i(T,\boldsymbol{\sigma}) \equiv \left.\frac{\partial F(T,\boldsymbol{\epsilon})}{\partial\epsilon_i}\right|_{\tilde{\boldsymbol{\epsilon}}(T,\boldsymbol{\sigma})}. \qquad (46)$$

For $C_{ij}^{\mathrm{adi}}(T,\boldsymbol{\sigma})$, the same equation holds, though $\mathcal{C}_{ij}^{\mathrm{adi}}(T,\boldsymbol{\sigma})$ and $s_i^{\mathrm{adi}}(T,\boldsymbol{\sigma})$ must be used, and the former is given by [22]

$$\mathcal{C}_{ij}^{\mathrm{adi}}(T,\boldsymbol{\sigma}) = \mathcal{C}_{ij}(T,\boldsymbol{\sigma}) + \frac{T}{c(\tilde{\boldsymbol{\epsilon}}(T,\boldsymbol{\sigma}),T)} \times$$
$$\left.\frac{\partial^2 F(T,\boldsymbol{\epsilon})}{\partial\epsilon_i\partial T}\right|_{\tilde{\boldsymbol{\epsilon}}(T,\boldsymbol{\sigma})} \left.\frac{\partial^2 F(T,\boldsymbol{\epsilon})}{\partial\epsilon_j\partial T}\right|_{\tilde{\boldsymbol{\epsilon}}(T,\boldsymbol{\sigma})}, \qquad (47)$$

where the heat capacity is given by

$$c(\tilde{\boldsymbol{\epsilon}}(T,\boldsymbol{\sigma}),T) = -T \left.\frac{\partial^2 F(T,\boldsymbol{\epsilon})}{\partial T^2}\right|_{\tilde{\boldsymbol{\epsilon}}(T,\boldsymbol{\sigma})}, \qquad (48)$$

and a similar derivation for s yields

$$s_i^{\mathrm{adi}}(T,\boldsymbol{\sigma}) = s_i(T,\boldsymbol{\sigma}) + \frac{T}{c(\tilde{\boldsymbol{\epsilon}}(T,\boldsymbol{\sigma}),T)} \left.\frac{\partial F(T,\boldsymbol{\epsilon})}{\partial T}\right|_{\tilde{\boldsymbol{\epsilon}}(T,\boldsymbol{\sigma})} \left.\frac{\partial^2 F(T,\boldsymbol{\epsilon})}{\partial\epsilon_i\partial T}\right|_{\tilde{\boldsymbol{\epsilon}}(T,\boldsymbol{\sigma})}. \qquad (49)$$

1. Results for cubic crystals

For the special case of cubic crystals under constant pressure, a variety of useful relations can be derived. Equation 44 reduces to

$$C_{ij}^{\mathrm{iso}}(T,\boldsymbol{\sigma}(P)) = \frac{\mathcal{C}_{ij}(T,\boldsymbol{\sigma}(P))}{|\hat{\mathbf{a}}_o|(1+\frac{1}{\sqrt{3}}\epsilon_{A_{1g}}(T,\boldsymbol{\sigma}(P)))}$$
$$+ \frac{P}{2}\mathrm{tr}\left(\hat{\boldsymbol{\lambda}}_i\hat{\boldsymbol{\lambda}}_j + \hat{\boldsymbol{\lambda}}_j\hat{\boldsymbol{\lambda}}_i\right), \qquad (50)$$

where we used

$$\frac{\partial^2\epsilon_{A_{1g}}}{\partial\eta_i\partial\eta_j} = -\frac{1}{2\sqrt{3}}(1+\frac{1}{\sqrt{3}}\epsilon_{A_{1g}})^{-3}\mathrm{tr}\left(\hat{\boldsymbol{\lambda}}_i\hat{\boldsymbol{\lambda}}_j + \hat{\boldsymbol{\lambda}}_j\hat{\boldsymbol{\lambda}}_i\right), \qquad (51)$$

which can be derived from equations 13 and 14. Eq. 50 can be expanded to leading order in P at an arbitrary temperature T as

$$C_{ij}^{\mathrm{iso}}(T,\boldsymbol{\sigma}(P)) = C_{ij}^{\mathrm{iso}}(T,\mathbf{0}) + P\left(\frac{\mathcal{C}_{ij}(T,\mathbf{0})}{\mathcal{C}_{A_{1g}A_{1g}}(T,\mathbf{0})}\right.$$
$$- (\sqrt{3}+\tilde{\epsilon}_{A_{1g}}(T,\mathbf{0})) \times \frac{\mathcal{C}_{ijA_{1g}}(T,\mathbf{0})}{\mathcal{C}_{A_{1g}A_{1g}}(T,\mathbf{0})} +$$
$$\left.\frac{1}{2}\mathrm{tr}\left(\hat{\boldsymbol{\lambda}}_i\hat{\boldsymbol{\lambda}}_j + \hat{\boldsymbol{\lambda}}_j\hat{\boldsymbol{\lambda}}_i\right)\right) + \dots, \qquad (52)$$

where

$$\mathcal{C}_{ijA_{1g}}(T,\boldsymbol{\sigma}) \equiv \left.\frac{\partial^3 F(T,\boldsymbol{\epsilon})}{\partial\epsilon_i\partial\epsilon_j\partial\epsilon_{A_{1g}}}\right|_{\tilde{\boldsymbol{\epsilon}}(T,\boldsymbol{\sigma})}, \qquad (53)$$

where we used the leading order expression Eq. 30. Using equations 29, 32, and 34, the bulk modulus, defined as the negative volume times the derivative of the pressure with respect to the volume, can be written as

$$B_{\mathrm{iso}}(T,P) = \frac{1}{3}C_{A_{1g}A_{1g}}^{\mathrm{iso}}(T,\boldsymbol{\sigma}(P)) + \frac{1}{3}P, \qquad (54)$$

The small strain approximation (SSA) (see Section II C 1) for $C_{ij}^{\mathrm{iso}}(T,\boldsymbol{\sigma}(P))$ can be evaluated using the third order Taylor series expansion of $F(T,\boldsymbol{\epsilon})$ in strain and evaluating Eq. 50, yielding $C_{ij}^{\mathrm{iso}(2)}(T,\boldsymbol{\sigma}(P))$. Retaining all terms yields a long equation, and therefore we only retain a subset of terms such that when the SSA is evaluated within the generalized QHA, the classical limit will

exactly recover the leading order expansion of the classical generalized QHA given in Eq. 90, yielding

$$C_{ij}^{\star\text{iso}}(T, \boldsymbol{\sigma}(P)) = \frac{1}{|\hat{\mathbf{a}}_o|}\left(F_{ij}(T) + \frac{-\dot{F}(T)}{\ddot{F}(T) - \frac{2}{\sqrt{3}}\dot{F}(T)} \times\right.$$

$$(\dot{F}_{ij}(T) - \frac{1}{\sqrt{3}}F_{ij}(T))\Big) + P\left(\frac{F_{ij}(T)}{\ddot{F}(T)} - \sqrt{3}\frac{\dot{F}_{ij}(T)}{\ddot{F}(T)} + \right.$$

$$\left.\frac{1}{2}\operatorname{tr}\left(\hat{\boldsymbol{\lambda}}_i\hat{\boldsymbol{\lambda}}_j + \hat{\boldsymbol{\lambda}}_j\hat{\boldsymbol{\lambda}}_i\right)\right), \tag{55}$$

where

$$F_{ij}(T) \equiv \left.\frac{\partial^2 F(T, \boldsymbol{\epsilon})}{\partial\epsilon_i\epsilon_j}\right|_{\boldsymbol{\epsilon}=\mathbf{0}}, \quad \dot{F}_{ij}(T) \equiv \left.\frac{\partial^3 F(T, \boldsymbol{\epsilon})}{\partial\epsilon_i\epsilon_j\partial\epsilon_{A_{1g}}}\right|_{\boldsymbol{\epsilon}=\mathbf{0}}, \tag{56}$$

and the superscript $\star$ denotes that this SSA was not uniformly truncated. Evaluating Eq. 55 within the generalized QHA can be seen as a generalization of the approximate expression for the bulk modulus in Ref. [3] (see Section III A 1 for further discussion).

In this study, elastic wave propagation is evaluated along the $\mathbf{Q}$ directions $(1, 0, 0)$ and $(3, 1, 1)$ for a cubic crystal. The point group of an arbitrary $\mathbf{Q}$ along the $(1, 0, 0)$ direction is C_{4v}, and the square of the velocities are given as

$$v_{(1,0,0)}^{A_1}(T, \boldsymbol{\sigma})^2 = |\hat{\mathbf{a}}(T, \boldsymbol{\sigma})|\frac{C_{11}}{m}, \tag{57}$$

$$v_{(1,0,0)}^{E^0}(T, \boldsymbol{\sigma})^2 = v_{(1,0,0)}^{E^1}(T, \boldsymbol{\sigma})^2 = |\hat{\mathbf{a}}(T, \boldsymbol{\sigma})|\frac{C_{44}}{m}, \tag{58}$$

while for an arbitrary $\mathbf{Q}$ along the $(3, 1, 1)$ direction, the point group is the order two group and the resulting square of the velocities are

$$v_{(3,1,1)}^{A_\pm}(T, \boldsymbol{\sigma})^2 = \frac{|\hat{\mathbf{a}}(T, \boldsymbol{\sigma})|}{22m}(10C_{11} + C_{12} + 13C_{44} \pm J), \tag{59}$$

$$v_{(3,1,1)}^{B}(T, \boldsymbol{\sigma})^2 = \frac{|\hat{\mathbf{a}}(T, \boldsymbol{\sigma})|}{11m}(C_{11} - C_{12} + 9C_{44}), \tag{60}$$

where

$$J^2 = 16C_{11}(4C_{11} - C_{12} + 9C_{44}) + 73(C_{12})^2 + 162C_{12}C_{44} + 153(C_{44})^2, \tag{61}$$

where the temperature and stress dependence of $C_{ij}(T, \boldsymbol{\sigma})$ has been suppressed for all velocity equations for brevity.

III. GENERALIZED QUASIHARMONIC APPROXIMATION

A. Formulation of the generalized QHA

The Born-Oppenheimer potential $\mathcal{V}(\boldsymbol{\epsilon}, \mathbf{u})$ can be constructed as a function of the Biot strains $\boldsymbol{\epsilon}$ and the nuclear displacements $\mathbf{u}$ (see Sections II A and II B for detailed definitions). The generalized QHA retains full

strain dependence of $\mathcal{V}(\boldsymbol{\epsilon}, \mathbf{u})$ while truncating the displacement dependence at second order, exactly evaluates $F(T, \boldsymbol{\epsilon})$ within this truncation, and evaluates observables at constant temperature and true stress (see Sections II C and II D). The only approximation within the generalized QHA is $\mathcal{V}(\boldsymbol{\epsilon}, \mathbf{u}) \approx \mathcal{V}_{qh}(\boldsymbol{\epsilon}, \mathbf{u})$, where

$$\mathcal{V}_{qh}(\boldsymbol{\epsilon}, \mathbf{u}) \equiv \mathcal{V}(\boldsymbol{\epsilon}, \mathbf{0}) + \frac{1}{2N}\sum_{ij\mathbf{q}}D_{\mathbf{q}}^{ij}(\boldsymbol{\epsilon})u_{\tilde{\mathbf{q}}}^{(i)}u_{\mathbf{q}}^{(j)}, \tag{62}$$

where $\mathcal{V}(\boldsymbol{\epsilon}, \mathbf{0})$ is the elastic energy, N is the number of $\mathbf{q}$-points in the first Brillouin zone, and $D_{\mathbf{q}}^{ij}(\boldsymbol{\epsilon})$ is the dynamical matrix at a strain $\boldsymbol{\epsilon}$ defined as

$$D_{\mathbf{q}}^{ij}(\boldsymbol{\epsilon}) \equiv \left.\frac{\partial^2\mathcal{V}(\boldsymbol{\epsilon}, \mathbf{u})}{\partial u_{\tilde{\mathbf{q}}}^{(i)}\partial u_{\mathbf{q}}^{(j)}}\right|_{\mathbf{u}=0}. \tag{63}$$

The generalized Helmholtz free energy $F(T, \boldsymbol{\epsilon})$ of the crystal can now be evaluated within the generalized QHA, where $\mathcal{V}(\boldsymbol{\epsilon}, \mathbf{u}) \approx \mathcal{V}_{qh}(\boldsymbol{\epsilon}, \mathbf{u})$. Given that $\mathcal{V}_{qh}(\boldsymbol{\epsilon}, \mathbf{u})$ is quadratic in displacements, the free energy $F_{qh}(T, \boldsymbol{\epsilon})$ per unit cell can be evaluated in closed form at a given temperature T and strain $\boldsymbol{\epsilon}$ as [53] (see Appendix B for additional discussion)

$$F_{qh}(T, \boldsymbol{\epsilon}) = \mathcal{V}(\boldsymbol{\epsilon}, \mathbf{0}) + F_o(T, \boldsymbol{\epsilon}), \tag{64}$$

$$F_o(T, \boldsymbol{\epsilon}) = \frac{1}{N}\sum_{\mathbf{q}\ell}\left(\frac{\hbar\omega_{\mathbf{q}\ell}(\boldsymbol{\epsilon})}{2} - k_B T\ln(1 + n_{\mathbf{q}\ell})\right), \tag{65}$$

where k_B is the Boltzmann constant, $n_{\mathbf{q}\ell}(T, \boldsymbol{\epsilon}) = [\exp(\hbar\omega_{\mathbf{q}\ell}(\boldsymbol{\epsilon})/k_B T) - 1]^{-1}$ is the Bose-Einstein distribution (the arguments of $n_{\mathbf{q}\ell}$ are suppressed throughout), and the phonon frequencies $\omega_{\mathbf{q}\ell}(\boldsymbol{\epsilon})$ are obtained by solving the generalized eigenvalue problem

$$\hat{\mathbf{D}}_{\mathbf{q}}(\boldsymbol{\epsilon})|\psi_{\mathbf{q}\ell}(\boldsymbol{\epsilon})\rangle = \hat{\mathbf{M}}\omega_{\mathbf{q}\ell}^2(\boldsymbol{\epsilon})|\psi_{\mathbf{q}\ell}(\boldsymbol{\epsilon})\rangle, \tag{66}$$

where ℓ is the band index and $\hat{\mathbf{M}}$ is the mass matrix.

The main task of the generalized QHA is then to obtain $\tilde{\boldsymbol{\epsilon}}(T, \boldsymbol{\sigma})$ by inverting Eq. 24, which requires the first derivative of the free energy, given as

$$\frac{\partial F_{qh}(T, \boldsymbol{\epsilon})}{\partial\epsilon_i} = \frac{\partial\mathcal{V}(\boldsymbol{\epsilon})}{\partial\epsilon_i} + \frac{\partial F_o(T, \boldsymbol{\epsilon})}{\partial\epsilon_i}, \tag{67}$$

where

$$\frac{\partial F_o(T, \boldsymbol{\epsilon})}{\partial\epsilon_i} = \frac{\hbar}{N}\sum_{\mathbf{q}\ell}(n_{\mathbf{q}\ell} + \frac{1}{2})\frac{\partial\omega_{\mathbf{q}\ell}(\boldsymbol{\epsilon})}{\partial\epsilon_i} \tag{68}$$

$$= -\frac{\hbar}{N}\sum_{\mathbf{q}\ell}(n_{\mathbf{q}\ell} + \frac{1}{2})\omega_{\mathbf{q}\ell}(\boldsymbol{\epsilon})\gamma_{i,\mathbf{q}\ell}(\boldsymbol{\epsilon}), \tag{69}$$

where $\gamma_{i,\mathbf{q}\ell}$ is the generalized Gruneisen parameter

$$\gamma_{i,\mathbf{q}\ell}(\boldsymbol{\epsilon}) \equiv -\left.\frac{\partial\ln(\omega_{\mathbf{q}\ell}(\boldsymbol{\epsilon}))}{\partial\epsilon_i}\right|_{\boldsymbol{\epsilon}}. \tag{70}$$

Within some strain parametrization, Eq. 67 is substituted into Eq. 24 in order to evaluate $\tilde{\boldsymbol{\epsilon}}(T, \boldsymbol{\sigma})$. The strain derivatives of the frequencies used to evaluate Eq. 68 are naturally obtained by Fourier interpolating the strain derivatives of the dynamical matrices and using eigenvalue perturbation theory (see Ref. [51], Section SII).

The second derivatives of the Helmholtz free energy are needed when constructing observables such as the thermal expansion and the elastic constants (see Sections II C and II D), and we enumerate the second derivatives within the generalized QHA. The second strain derivative is given as

$$\frac{\partial^2 F_{qh}(T, \boldsymbol{\epsilon})}{\partial \epsilon_i \partial \epsilon_j} = \frac{\partial^2 \mathcal{V}(\boldsymbol{\epsilon}, \mathbf{0})}{\partial \epsilon_i \partial \epsilon_j} + \frac{\partial^2 F_o(T, \boldsymbol{\epsilon})}{\partial \epsilon_i \partial \epsilon_j}, \qquad (71)$$

where

$$\frac{\partial^2 F_o(T, \boldsymbol{\epsilon})}{\partial \epsilon_i \partial \epsilon_j} = \frac{\hbar}{N} \sum_{\mathbf{q}\ell} \left(\frac{\partial^2 \omega_{\mathbf{q}\ell}(\boldsymbol{\epsilon})}{\partial \epsilon_i \partial \epsilon_j} (n_{\mathbf{q}\ell} + \frac{1}{2}) - \right.$$

$$\left. \frac{\hbar(n_{\mathbf{q}\ell} + 1) n_{\mathbf{q}\ell}}{k_B T} \frac{\partial \omega_{\mathbf{q}\ell}(\boldsymbol{\epsilon})}{\partial \epsilon_i} \frac{\partial \omega_{\mathbf{q}\ell}(\boldsymbol{\epsilon})}{\partial \epsilon_j} \right) \qquad (72)$$

$$= \frac{1}{N} \sum_{\mathbf{q}\ell} \left((\gamma_{i,\mathbf{q}\ell}(\boldsymbol{\epsilon}) \gamma_{j,\mathbf{q}\ell}(\boldsymbol{\epsilon}) - \frac{\partial \gamma_i(\boldsymbol{\epsilon})}{\partial \epsilon_j}) \hbar \omega_{\mathbf{q}\ell}(\boldsymbol{\epsilon}) (n_{\mathbf{q}\ell} + \frac{1}{2}) \right.$$

$$\left. - T c_{\mathbf{q}\ell}(T, \boldsymbol{\epsilon}) \gamma_{i,\mathbf{q}\ell}(\boldsymbol{\epsilon}) \gamma_{j,\mathbf{q}\ell}(\boldsymbol{\epsilon}) \right), \qquad (73)$$

where $c_{\mathbf{q}\ell}$ is the modal heat capacity, defined as

$$c_{\mathbf{q}\ell}(T, \boldsymbol{\epsilon}) \equiv \frac{\hbar^2 \omega_{\mathbf{q}\ell}^2(\boldsymbol{\epsilon})}{k_B T^2} n_{\mathbf{q}\ell}(n_{\mathbf{q}\ell} + 1). \qquad (74)$$

The cross derivative between temperature and strain is given as

$$\frac{\partial^2 F_{qh}(T, \boldsymbol{\epsilon})}{\partial \epsilon_i \partial T} = \frac{1}{N} \sum_{\mathbf{q}\ell} \frac{\hbar^2 \omega_{\mathbf{q}\ell}(\boldsymbol{\epsilon})}{k_B T^2} n_{\mathbf{q}\ell}(n_{\mathbf{q}\ell} + 1) \frac{\partial \omega_{\mathbf{q}\ell}(\boldsymbol{\epsilon})}{\partial \epsilon_i} \qquad (75)$$

$$= \frac{-1}{N} \sum_{\mathbf{q}\ell} \gamma_{i,\mathbf{q}\ell}(\boldsymbol{\epsilon}) c_{\mathbf{q}\ell}(T, \boldsymbol{\epsilon}). \qquad (76)$$

Finally, we have the second derivative with respect to temperature, given as

$$\frac{\partial^2 F_{qh}(T, \boldsymbol{\epsilon})}{\partial T^2} = -\frac{1}{NT} \sum_{\mathbf{q}\ell} c_{\mathbf{q}\ell}(T, \boldsymbol{\epsilon}). \qquad (77)$$

1. Results for cubic crystals

For the case of a cubic crystal within the generalized QHA, all of the formal quantities defined in Sections II C 1 and II D 1 can be obtained by substituting

$F(T, \boldsymbol{\epsilon}) \rightarrow F_{qh}(T, \boldsymbol{\epsilon})$. The A_{1g} stress as a function of temperature and A_{1g} strain from Eq. 29 yields

$$\tilde{\sigma}_{A_{1g}}(T, \boldsymbol{\epsilon}(\epsilon_{A_{1g}})) = \frac{1}{|\hat{\mathbf{a}}_o|(1 + \frac{1}{\sqrt{3}}\epsilon_{A_{1g}})^2} \times$$

$$\left(\frac{\partial \mathcal{V}(\boldsymbol{\epsilon}, \mathbf{0})}{\partial \epsilon_{A_{1g}}} \bigg|_{\boldsymbol{\epsilon}(\epsilon_{A_{1g}})} + \frac{\partial F_o(T, \boldsymbol{\epsilon})}{\partial \epsilon_{A_{1g}}} \bigg|_{\boldsymbol{\epsilon}(\epsilon_{A_{1g}})} \right). \qquad (78)$$

The strain map $\tilde{\epsilon}_{A_{1g}}^{(1)}(T, \boldsymbol{\sigma}(\sigma_{A_{1g}}))$ defined in Eq. 37, which is obtained from a small strain approximation, evaluates to

$$\tilde{\epsilon}_{A_{1g}}^{(1)}(T, \boldsymbol{\sigma}(\sigma_{A_{1g}})) = \frac{|\hat{\mathbf{a}}_o|\sigma_{A_{1g}} - \dot{F}_o(T)}{\ddot{\mathcal{V}} + \ddot{F}_o(T) - \frac{2}{\sqrt{3}}\dot{F}_o(T)}, \qquad (79)$$

where

$$\dot{F}_o(T) \equiv \frac{\partial F_o(T, \boldsymbol{\epsilon})}{\partial \epsilon_{A_{1g}}} \bigg|_{\boldsymbol{\epsilon} = \mathbf{0}}, \qquad \ddot{\mathcal{V}} \equiv \frac{\partial^2 \mathcal{V}(\boldsymbol{\epsilon}, \mathbf{0})}{\partial \epsilon_{A_{1g}}^2} \bigg|_{\boldsymbol{\epsilon} = \mathbf{0}}, \qquad (80)$$

and $\ddot{F}_o(T)$ is defined correspondingly. Converting to volumetric strain using Eq. 32, we obtain

$$\tilde{\epsilon}_v^{(1)}(T, \mathbf{0}) = \frac{-F_o'(T)}{\mathcal{V}'' + F_o''(T)}, \qquad (81)$$

where the prime denotes the volumetric strain derivative at zero strain, analogous to Eq. 80. If $F_o''(T)$ is neglected in Eq. 81, the usual Gruneisen equation is recovered (see Eq. 20 in Ref. [3]).

A small strain approximation for the bulk modulus can be evaluated by substituting $C_{A_{1g}A_{1g}}^{\star\text{iso}}(T, \boldsymbol{\sigma}(P))$, defined in Eq. 55, into Eq. 54. To compare with previous literature, we convert to volumetric strain derivatives using Eq. 32, yielding

$$B_{\text{iso}}^\star(T, P) = \frac{1}{|\hat{\mathbf{a}}_o|} \left(\mathcal{V}'' + F_o''(T) - F_o'(T) \times \right.$$

$$\left(1 - \frac{\mathcal{V}''' + F_o'''(T)}{\mathcal{V}'' + F_o''(T)} \right) \right) + P \left(1 - \right.$$

$$\left. \frac{3(\mathcal{V}''' + F_o'''(T)) + 6(\mathcal{V}'' + F_o''(T)) + \frac{2}{3}F_o'(T)}{3(\mathcal{V}'' + F_o''(T)) + 2F_o'(T)} \right). \qquad (82)$$

Eq. 82 can be seen as the finite pressure generalization of Eq. 37 in Ref. [3], and equality is obtained by setting $P = 0$ and neglecting $F_o''(T)$ and $F_o'''(T)$ in the second line of Eq. 82.

B. The classical limit of the generalized QHA

It is useful to document the generalized QHA in the case of classical mechanics, which will yield the same results as the quantum case for sufficiently high temperatures. The classical Helmholtz free energy is

$$F_{qh}^{cl}(T, \boldsymbol{\epsilon}) = \mathcal{V}(\boldsymbol{\epsilon}, \mathbf{0}) + k_B T \Omega(\boldsymbol{\epsilon})$$

$$- 3n_a k_B T \ln\left(\frac{k_B T}{\hbar} \right), \qquad (83)$$

where

$$\Omega(\boldsymbol{\epsilon}) = \frac{1}{N} \sum_{\mathbf{q}\ell} \ln(\omega_{\mathbf{q}\ell}(\boldsymbol{\epsilon})). \tag{84}$$

In order to obtain $\tilde{\boldsymbol{\epsilon}}(T, \boldsymbol{\sigma})$ from Eq. 24 and Eq. 25 within the classical generalized QHA, we evaluate

$$\frac{\partial F_{qh}^{cl}(T, \boldsymbol{\epsilon})}{\partial \boldsymbol{\epsilon}} = \frac{\partial \mathcal{V}(\boldsymbol{\epsilon}, \mathbf{0})}{\partial \boldsymbol{\epsilon}} + k_B T \frac{\partial \Omega(\boldsymbol{\epsilon})}{\partial \boldsymbol{\epsilon}}, \tag{85}$$

where

$$\frac{\partial \Omega(\boldsymbol{\epsilon})}{\partial \epsilon_i} = -\frac{1}{N} \sum_{\mathbf{q}\ell} \gamma_{i,\mathbf{q}\ell} \tag{86}$$

is the negative of the q-averaged generalized Gruneisen parameter. To connect with previous literature, it is also useful to define the mode averaged generalized Gruneisen parameter

$$\bar{\gamma}_i(\boldsymbol{\epsilon}) = -\frac{1}{3n_a} \left. \frac{\partial \Omega(\boldsymbol{\epsilon})}{\partial \epsilon_i} \right|_{\boldsymbol{\epsilon}}. \tag{87}$$

1.   Results for cubic crystals

For the case of a cubic crystal under constant pressure, the A_{1g} component of the classical true stress as a function of the A_{1g} strain and temperature is given as

$$\tilde{\sigma}_{A_{1g}}(T, \boldsymbol{\epsilon}(\epsilon_{A_{1g}})) = \frac{1}{|\hat{\mathbf{a}}_o|(1 + \frac{1}{\sqrt{3}}\epsilon_{A_{1g}})^2} \times$$
$$\left(\left. \frac{\partial \mathcal{V}(\boldsymbol{\epsilon}, \mathbf{0})}{\partial \epsilon_{A_{1g}}} \right|_{\boldsymbol{\epsilon}(\epsilon_{A_{1g}})} + k_B T \left. \frac{\partial \Omega(\boldsymbol{\epsilon})}{\partial \epsilon_{A_{1g}}} \right|_{\boldsymbol{\epsilon}(\epsilon_{A_{1g}})} \right). \tag{88}$$

The classical strain map $\tilde{\epsilon}_{A_{1g}}(T, \boldsymbol{\sigma}(P))$ can be written to second order in temperature and pressure by Taylor series expanding Eq. 88 to second order in the A_{1g} strain, solving for the A_{1g} strain, and Taylor series expanding the result to second order in temperature and pressure, yielding

$$\tilde{\epsilon}_{A_{1g}}(T, \boldsymbol{\sigma}(P)) = T \frac{-k_B \dot{\Omega}}{\ddot{\mathcal{V}}} + \frac{k_B^2}{2} T^2 \left(\frac{2\dot{\Omega}\ddot{\Omega}}{\ddot{\mathcal{V}}^2} - \frac{\dddot{\mathcal{V}}\dot{\Omega}^2}{\ddot{\mathcal{V}}^3} \right)$$
$$- \frac{\sqrt{3}|\hat{\mathbf{a}}_o|}{\ddot{\mathcal{V}}} P + PT \frac{\sqrt{3}k_B|\hat{\mathbf{a}}_o|}{\ddot{\mathcal{V}}^2} \left(\ddot{\Omega} + \dot{\Omega}(\frac{2\sqrt{3}}{3} - \frac{\dddot{\mathcal{V}}}{\ddot{\mathcal{V}}}) \right)$$
$$+ P^2 \frac{3|\hat{\mathbf{a}}_o|^2}{2\ddot{\mathcal{V}}^3} (\frac{4}{\sqrt{3}}\ddot{\mathcal{V}} - \dddot{\mathcal{V}}) + \dots, \tag{89}$$

where $\ddot{\mathcal{V}}$, $\dot{\Omega}$, $\ddot{\Omega}$ are constants defined correspondingly to Eq. 80. Equation 89 is encoded by 4 A_{1g} strain derivatives and can be seen as a finite pressure generalization of equations 32 and 33 in Ref. [3]; though Eq. 32 must be used to convert between A_{1g} and volumetric strains

to obtain equivalence. Similarly, the classical elastic constants can be written to first order in temperature and pressure using Eq. 52 as

$$C_{ij}^{\text{iso}}(T, \boldsymbol{\sigma}(P)) = \frac{\mathcal{V}_{ij}}{|\hat{\mathbf{a}}_o|} + T \frac{k_B}{|\hat{\mathbf{a}}_o|} \left(\Omega_{ij} + \frac{\dot{\Omega}\mathcal{V}_{ij}}{\sqrt{3}\ddot{\mathcal{V}}} - \frac{\dot{\Omega}\dot{\mathcal{V}}_{ij}}{\ddot{\mathcal{V}}} \right) +$$
$$P \left(\frac{1}{2} \text{tr}\left(\hat{\boldsymbol{\lambda}}_i \hat{\boldsymbol{\lambda}}_j + \hat{\boldsymbol{\lambda}}_j \hat{\boldsymbol{\lambda}}_i \right) + \frac{\mathcal{V}_{ij}}{\ddot{\mathcal{V}}} - \sqrt{3}\frac{\dot{\mathcal{V}}_{ij}}{\ddot{\mathcal{V}}} \right) + \dots, \tag{90}$$

where

$$\mathcal{V}_{ij} = \left. \frac{\partial^2 \mathcal{V}(\boldsymbol{\epsilon}, \mathbf{0})}{\partial \epsilon_i \partial \epsilon_j} \right|_{\boldsymbol{\epsilon}=\mathbf{0}}, \qquad \dot{\mathcal{V}}_{ij} = \left. \frac{\partial^3 \mathcal{V}(\boldsymbol{\epsilon}, \mathbf{0})}{\partial \epsilon_{A_{1g}} \partial \epsilon_i \partial \epsilon_j} \right|_{\boldsymbol{\epsilon}=\mathbf{0}}, \tag{91}$$

and where

$$\Omega_{ij} = \left. \frac{\partial^2 \Omega(\boldsymbol{\epsilon})}{\partial \epsilon_i \partial \epsilon_j} \right|_{\boldsymbol{\epsilon}=\mathbf{0}}. \tag{92}$$

Eq. 90 is encoded by five strain derivatives evaluated at zero strain. Inserting Eq. 90 into Eq. 54, the classical bulk modulus to leading order in temperature and pressure is obtained as

$$B_{\text{iso}}(T, P) = \frac{\ddot{\mathcal{V}}}{3|\hat{\mathbf{a}}_o|} + P(1 - \frac{1}{\sqrt{3}}\frac{\dddot{\mathcal{V}}}{\ddot{\mathcal{V}}})$$
$$+ T \frac{k_B}{3|\hat{\mathbf{a}}_o|} (\ddot{\Omega} + \frac{\dot{\Omega}}{\sqrt{3}} - \frac{\dot{\Omega}\dddot{\mathcal{V}}}{\ddot{\mathcal{V}}}) + \dots, \tag{93}$$

Eq. 93 can be seen as a finite pressure generalization of the classical limit of Eq. 37 in Ref. [3], though Eq. 32 must be used to convert between A_{1g} and volumetric strains to obtain equivalence.

C.   Parametrization of strain dependence within the generalized QHA

Within the generalized QHA, the elastic energy $\mathcal{V}(\boldsymbol{\epsilon}, \mathbf{0})$ and the dynamical matrix must be parametrized as a function of strain in order to evaluate these expressions. As emphasized in the introduction, there are two natural approaches for parametrizing the strain dependence: evaluation of a Taylor series expansion in strain or evaluation on a grid of strains which are then interpolated. Evaluation on a grid of strains requires a choice for the density of the strain grid points, which will set the balance of precision and efficiency. Furthermore, some interpolation scheme will be needed to obtain values at arbitrary strains. The other approach would be a Taylor

series in strain, whereby $\mathcal{V}_{qh}$ is expanded as

$$
\begin{aligned}
\mathcal{V}_{qh}(\boldsymbol{\epsilon}, \mathbf{u}) = {} & \mathcal{V}(\mathbf{0}, \mathbf{0}) + \frac{1}{2} \sum_{ij} \left.\frac{\partial^2 \mathcal{V}(\boldsymbol{\epsilon}, \mathbf{0})}{\partial \epsilon_i \partial \epsilon_j}\right|_{\boldsymbol{\epsilon}=\mathbf{0}} \epsilon_i \epsilon_j + \\
& \frac{1}{6} \sum_{ijk} \left.\frac{\partial^3 \mathcal{V}(\boldsymbol{\epsilon}, \mathbf{0})}{\partial \epsilon_i \partial \epsilon_j \partial \epsilon_k}\right|_{\boldsymbol{\epsilon}=\mathbf{0}} \epsilon_i \epsilon_j \epsilon_k + \\
& \frac{1}{2N} \sum_{ij\mathbf{q}} D_{\mathbf{q}}^{ij}(\mathbf{0}) u_{\bar{\mathbf{q}}}^{(i)} u_{\mathbf{q}}^{(j)} + \\
& \frac{1}{2N} \sum_{ijk\mathbf{q}} \left.\frac{\partial D_{\mathbf{q}}^{ij}(\boldsymbol{\epsilon})}{\partial \epsilon_k}\right|_{\boldsymbol{\epsilon}=\mathbf{0}} u_{\bar{\mathbf{q}}}^{(i)} u_{\mathbf{q}}^{(j)} \epsilon_k + \dots, \quad (94)
\end{aligned}
$$

where the expansion may be truncated at $\mathcal{N}$-th order, with $\mathcal{N}$ counting the combined number of strain and displacement derivatives in a given term. For $\mathcal{N} = 2$, we recover the usual harmonic approximation, while a truncation at order $\mathcal{N} \geq 3$ yields a nontrivial QHA. In our paper, we execute derivatives for $\mathcal{N} \leq 4$, and our expansion is written purely in terms of space group irreducible derivatives (see Ref. [51] Section SVII for explicit equations).

1. Generalized QHA using irreducible derivatives

The irreducible approach to the generalized QHA requires the computation of the elastic energy and the irreducible second order displacement derivatives (i.e., the irreducible components of the dynamical matrix) [55, 56] as a function of strain, which can be accomplished using a strain grid interpolation or a Taylor series. For the strain grid interpolation, the elastic energy $\mathcal{V}(\boldsymbol{\epsilon}, \mathbf{0})$ and the irreducible second order displacement derivatives $\{d_{\bar{\mathbf{q}}\mathbf{q}}^{\alpha\alpha'}(\boldsymbol{\epsilon})\}$, where α, α' label irreducible representations of the little group of $\mathbf{q}$, are computed at each strain grid point $\boldsymbol{\epsilon}$. For a Taylor series, the elastic energy is encoded by the irreducible strain derivatives of $\mathcal{V}(\boldsymbol{\epsilon}, \mathbf{0})$ up to order $\mathcal{N}$, denoted as $\{d_{\beta_1,\dots,\beta_{\mathcal{N}}}\}$ where β_i labels an irreducible representation of strain; and the strain dependence of the irreducible second order displacement derivatives is encoded using up to $\mathcal{N} - 2$ order strain derivatives of $\{d_{\bar{\mathbf{q}}\mathbf{q}}^{\alpha\alpha'}(\boldsymbol{\epsilon})\}$, denoted by $\{d_{\bar{\mathbf{q}}\mathbf{q}\beta_1,\dots,\beta_{\mathcal{N}-2}}^{\alpha\alpha'}\}$. In practice, the infinite crystal is approximated by a finite crystal, characterized by all translations within a symmetric supercell $\hat{\mathbf{S}}_{BZ}$ (i.e., supercells which are invariant to the point group) [56]. All irreducible derivatives within $\hat{\mathbf{S}}_{BZ}$ must then be computed, either with perturbative or finite displacement techniques, and then interpolated to the infinite crystal.

In our work, we use the lone irreducible derivative (LID) approach [56] to compute all irreducible second order displacement derivatives of the Born-Oppenheimer potential within $\hat{\mathbf{S}}_{BZ}$, and LID executes all calculations in supercells that have the smallest multiplicity allowed by group theory. For the face-centered cubic lattice, where $\hat{\mathbf{a}}_o = \frac{a_o}{2}(\hat{\mathbf{J}} - \hat{\mathbf{1}})$, two classes of $\hat{\mathbf{S}}_{BZ}$ are used in our

study: $n\hat{\mathbf{1}}$ (i.e., uniform supercells) and $n\hat{\mathbf{S}}_C = n(\hat{\mathbf{J}} - 2\hat{\mathbf{1}})$, where n is a positive integer, $\hat{\mathbf{1}}$ is the 3×3 identity matrix, and $\hat{\mathbf{J}}$ is a 3×3 matrix with each element being 1. It should be noted that $\hat{\mathbf{S}}_C$ yields the conventional cubic supercell. Uniform supercells have multiplicity n^3, and the LID approach can extract all irreducible derivatives from supercells with multiplicity less than or equal to n, in contrast to single supercell approaches which require n^3 [57]. Similarly, supercells of the class $n\hat{\mathbf{S}}_C$ have multiplicity $4n^3$, and the LID approach can extract all irreducible derivatives from supercells with multiplicity less than or equal to $2n$. Given the scaling of DFT calculations with system size, the LID approach results in a massive reduction in computational cost. Further reductions in cost can be realized by using the bundled irreducible derivative approach [56], but this was not pursued in the present study.

IV. EXPERIMENTAL METHODS

Thoria (ThO$_2$) single crystals were grown using the hydrothermal synthesis technique [58] (see reference [59] for additional details). Crystallographic orientations were identified from the crystal morphology and the angle between faces. A resulting thoria crystal was characterized using X-ray diffraction (XRD), which was performed at room temperature using a Rigaku XtaLab Mini equipped with Mo Kα radiation (λ= 0.71073 Å). A full diffraction data set was collected using $\phi=0°$, 120°, and 240°, with 2θ from -60° to 120° with a 1° step. Crystal Clear software was used for data integration and the structure was solved by direct methods using Shelxtl-97 [60] and refined by least-squares techniques; a final R1 of 0.0378 was obtained for the crystal structure. Further characterization was performed using μ-Raman measurements and time-of-flight secondary ion mass spectrometry to ensure the crystal quality (see the Supplementary material in Ref. [61]), resulting in crystals of equivalent quality to previous growths [58].

Time-of-flight inelastic neutron scattering measurements were performed using the Hybrid Spectrometer (HYSPEC) at the Spallation Neutron Source at Oak Ridge National Laboratory, with an incoming energy of 17 meV. The ThO$_2$ sample used for INS in the present study was also used in our previously reported measurements[61]. The transverse acoustic mode along the Γ to X_z direction scatters strongly near the Γ point $(2, 2, 0)$, in units of $2\pi/a$, which allows for the extraction of the speed of sound and the C_{44} values as a function of temperature. The observed inelastic neutron scattering (INS) is analyzed as a function of energy for fixed values of $\mathbf{Q}$, where the peak of the scattering function yields a value of energy E. The peak fitting is repeated for several observable $\mathbf{Q}$ values $(2, 2, \zeta)$, in units of $2\pi/a$, and the resulting dispersion is fit to the equation $E = \hbar v_T \zeta$ to determine v_T, the speed of sound of the transverse acoustic mode. Given v_T, we calculate $C_{44} = \rho v_T^2$, where

ρ is the material density measured by INS.

Time-domain Brillouin Scattering (TDBS) [62, 63] was used to generate picosecond duration coherent acoustic phonons that propagate in the depth normal to the sample surface by irradiating the sample with ultrashort pump laser pulses. Two thoria crystals were utilized for TDBS measurements: one with an exposed (1,0,0) plane and another with a (3,1,1) plane. The (1,0,0) and (3,1,1) surfaces of the thoria crystals were coated with an approximately 7 nm thick gold film to ensure strong optical absorption of the pump laser beam. Generation of coherent acoustic phonons was accomplished via thermoelastic expansion of the gold film following absorption of the pump laser pulse energy. A time-delayed probe laser pulse was used to detect changes in optical reflectivity of the gold film induced by the propagating acoustic phonon modes via photoelastic coupling. The ultrasonic velocity of the coherent phonon modes v was calculated from the frequency of the measured time-resolved reflectivity f changes using the relation [64–66],

$$v = \frac{f\lambda}{2n}, \tag{95}$$

where λ is the optical wavelength of the probe laser beam, and n is the real part of the refractive index of thoria. The frequency of the coherent acoustic mode was determined by fitting a Gaussian function to the peaks in the Fourier spectrum of the time-domain signal (see Ref. [51] Section SI). The longitudinal acoustic mode with velocity $v_{(1,0,0)}^{A_1}$ was detected along the (1,0,0) direction, while the quasi-longitudinal and fast transverse acoustic modes, with velocities $v_{(3,1,1)}^{A_+}$ and $v_{(3,1,1)}^{A_-}$, respectively, were detected along the (3,1,1) orientation. For the (1,0,0) thoria crystal, TDBS signals were acquired between 77 K and 350 K by placing the samples in a temperature-controlled, liquid nitrogen-cooled cryostat. The TDBS measurements on the (3,1,1) thoria crystal are only reported for $T = 77$ K.

In the $(1, 0, 0)$ direction, the longitudinal velocity yields $C_{11} = 4m(v_{(1,0,0)}^{A_1})^2/a^3$, where $m = m_{\mathrm{Th}} + 2m_{\mathrm{O}}$ and a is the experimental lattice parameter of the conventional cubic cell. In the $(3, 1, 1)$ direction, the quasi-longitudinal velocity $v_{(3,1,1)}^{A_+}$ and the fast transverse velocity $v_{(3,1,1)}^{A_-}$ can then be used, along with $v_{(1,0,0)}^{A_1}$, to construct the other independent elastic constants as

$$\begin{aligned} C_{12} = \frac{m}{59a^3}\Big(&- 225((v_{(3,1,1)}^{A_-})^2 + (v_{(3,1,1)}^{A_+})^2) + \\ &214(v_{(1,0,0)}^{A_1})^2 + 13J\Big), \end{aligned} \tag{96}$$

$$\begin{aligned} C_{44} = \frac{m}{59a^3}\Big(&217((v_{(3,1,1)}^{A_-})^2 + (v_{(3,1,1)}^{A_+})^2) - \\ &198(v_{(1,0,0)}^{A_1})^2 - J\Big), \end{aligned} \tag{97}$$

$$\begin{aligned} J^2 = &361(v_{(3,1,1)}^{A_-})^4 - 1874(v_{(3,1,1)}^{A_-})^2(v_{(3,1,1)}^{A_+})^2 + \\ &361(v_{(3,1,1)}^{A_+})^4 + 1152((v_{(1,0,0)}^{A_1})^2((v_{(3,1,1)}^{A_-})^2 + \\ &(v_{(3,1,1)}^{A_+})^2) - (v_{(1,0,0)}^{A_1})^4). \end{aligned} \tag{98}$$

All of the above quantities depend on the experimentally chosen temperature and stress, where the temperatures used in our study range from $T = 77$ K to $T = 350$ K and the stress is $\boldsymbol{\sigma} = \mathbf{0}$.

V. COMPUTATION DETAILS

Density functional theory (DFT) calculations were performed using the projector augmented wave (PAW) method [67, 68], as implemented in the Vienna *ab initio* simulation package (VASP) [69–72]. Results were generated using three different exchange-correlation functionals: the local density approximation (LDA) [73], generalized gradient approximation (GGA) [74], and strongly constrained and appropriately normed (SCAN) [75] functional. Following previous conventions (see reference [76] for details), SCAN calculations employ PAW potentials generated using the Perdew, Burke, Ernzerhof GGA functional [77] (VASP.5.2 version). In all cases, thorium and soft oxygen PAW potentials were employed. A plane wave basis with a kinetic energy cutoff of 800 eV was used. A Γ-centered **k**-point mesh of $20\times20\times20$ was used for the primitive unit cell, and corresponding mesh densities were used for supercells. Convergence of phonons and phonon strain derivatives were verified by testing plane-wave cutoff energies up to 1000 eV and **k**-point meshes up to $30\times30\times30$. Strain and displacement derivatives were computed using the lone irreducible derivative approach [56] with the central finite difference method (see Section III C 1 for further details). Quadratic error tails were constructed in order to extrapolate to the limit of zero amplitude. All atomic displacement amplitudes used for displacement derivative calculations employed 10 equally spaced steps of variable size within the range 0.01-0.2 Å. Strain derivatives of phonons used strains of 0.02-0.20 with steps of 0.02. The strain derivatives of the elastic energy used strains of 0.01-0.1 with steps of 0.01. When utilizing the strain grid interpolation approach, the elastic energy and the irreducible second order displacement derivatives were evaluated at volumetric strain increments of 0.01.

X-C	a_o	C_{11}	C_{12}	C_{44}	ϵ^∞	Z^*_{Th}	Z^*_O
LDA	5.531	383.8	129.6	87.0	4.88	5.41	-2.70
						5.39^d	-2.70^d
SCAN	5.592	375.9	116.6	82.4	4.46	5.62	-2.50
PW91	5.621	352.7	108.1	72.0	4.79	5.39	-2.70
	5.62^a	349.5^a	111.4^a	70.6^a			
PBE	5.619^b	351.2^b	106.9^b	74.1^b	4.83^b	5.41^b	-2.71^b
	5.61^c	351.9^c	105.4^c	70.9^c			
WC	5.56^c	370.9^c	118.7^c	80.8^c			
PBEsol	5.55^c	370.6^c	119.3^c	80.7^c		5.37^d	-2.68^d

^{a} Ref. [34], ^{b} Ref. [33], ^{c} Ref. [30], ^{d} Ref.[32]

TABLE I. Classical QHA results at $T = 0$, $\boldsymbol{\sigma} = 0$ for the lattice parameter (Å) and the elastic constants (GPa); the dielectric constant and Born effective charges computed using various exchange-correlation functionals (X-C). Comparisons with previous publications are provided where available.

When approximating integrals over the Brillouin zone, phonons were Fourier interpolated [56] to $\hat{\mathbf{S}}_{BZ} = 10\hat{\mathbf{1}}$ for all QHA calculations. For computing the phonon and Gruneisen density of states (DOS), integrals were performed using the tetrahedron method [78]. The dielectric tensor and Born effective charges were calculated from density functional perturbation theory[79, 80] for LDA and GGA, and finite electric fields were used for SCAN. The relaxed lattice parameters a_o (i.e., the classical QHA result at $T = 0$, $\boldsymbol{\sigma} = \mathbf{0}$), the second strain derivatives of $\mathcal{V}(\boldsymbol{\epsilon}, \mathbf{0})$ evaluated at a_o, dielectric constants, and Born effective charges (BEC) are presented in Table I, along with results from the literature.

The LO-TO splitting can be incorporated within the LID approach using the method outlined in Gonze et al. [81] (see Appendix A). When using the strain grid interpolation, the LO-TO splitting is computed at each strain value in the interpolation. When evaluating the Taylor series expansion in strain, the strain derivative of the LO-TO splitting contribution must also be evaluated (see Appendix A and Ref. [51] Section SV for explicit equations).

VI. RESULTS AND DISCUSSION

In both the strain grid interpolation and Taylor series approaches, the irreducible second order displacement derivatives $d_{\bar{\mathbf{q}}\mathbf{q}}^{\alpha\alpha'}$ will be computed at zero strain (i.e., at $\hat{\mathbf{a}}_o$), and we begin by presenting them (our notation follows Ref. [56]). For clarity, we focus our discussion around $\hat{\mathbf{S}}_{BZ} = \hat{\mathbf{S}}_C$, though larger supercells will need to be evaluated in order to determine supercell convergence. Remarkably, we later demonstrate that $\hat{\mathbf{S}}_C$ achieves sufficient convergence within the QHA, such that only a small number of irreducible derivatives are required. The discrete irreducible Brillouin zone associated with $\hat{\mathbf{S}}_C$ can

be chosen as $\tilde{q}_{IBZ} = \{\Gamma, X_z\}$ [56]. Symmetrizing the displacement vectors at the Γ point according to the irreducible representations of O_h yields $T_{1u} \oplus T_{2g}$, and we have explicitly excluded the T_{1u} acoustic modes which guarantees that the acoustic sum rules are satisfied by construction. For the X_z-point, the little group is D_{4h} and symmetrizing yields $A_{1g} \oplus B_{1u} \oplus A_{2u} \oplus E_g \oplus 2E_u$. The great orthogonality theorem [55] dictates that there are two irreducible derivatives at the Γ point and seven irreducible derivatives at the X-point, as shown in Table II (see Ref. [51] for irreducible derivatives in supercells up to $4\hat{\mathbf{1}}$ in Table SIV). It should be noted that the space group of ThO_2 allows a phase convention which yields purely real irreducible derivatives.

The irreducible second order displacement derivatives $d_{\bar{\mathbf{q}}\mathbf{q}}^{\alpha\alpha'}$ yield the dynamical matrix in block diagonal form for the finite translation group. Subsequently, Fourier interpolation can be used to interpolate to a denser grid of $\mathbf{q}$-points, and the resulting dynamical matrices can be diagonalized, yielding the phonons; and allowing for the evaluation of the partition function. We showcase the phonon dispersion and density-of-states (DOS) for $\hat{\mathbf{S}}_{BZ} = 4\hat{\mathbf{1}}$ (see Figure 1, panel a, and Ref. [51] for definition of $\mathbf{q}$-points). There is good agreement with experimental measurements [41, 61] for all functionals, and SCAN appears to be the best overall.

For the strain grid interpolation approach to the QHA, the elastic energy and $d_{\bar{\mathbf{q}}\mathbf{q}}^{\alpha\alpha'}$ are simply recomputed at each strain (see Ref. [51], Table SII), yielding all necessary irreducible information to solve the QHA equations. For the Taylor series approach, we compute the first and second order irreducible strain derivatives of $d_{\bar{\mathbf{q}}\mathbf{q}}^{\alpha\alpha'}$, denoted $d_{\bar{\mathbf{q}}\mathbf{q}\beta}^{\alpha\alpha'}$ and $d_{\bar{\mathbf{q}}\mathbf{q}\beta_1\beta_2}^{\alpha\alpha'}$, in addition to computing up to fourth order irreducible strain derivatives of the elastic energy (i.e., $d_{\beta_1\beta_2}$, $d_{\beta_1\beta_2\beta_3}$, and $d_{\beta_1\beta_2\beta_3\beta_4}$). The strain can be decomposed into the symmetrized strains $A_{1g} \oplus E_g \oplus T_{2g}$ for O_h, and to $2A_{1g} \oplus B_{1g} \oplus B_{2g} \oplus E_g$ for D_{4h}. Given our phase conventions for X_z, the symmetry lineage for $O_h \rightarrow D_{4h}$ yields

$$A_{1g} \rightarrow A_{1g}, \quad E_g^0 \rightarrow B_{1g}, \quad E_g^1 \rightarrow {}^1A_{1g}$$
$$T_{2g}^0 \rightarrow B_{2g}, \quad T_{2g}^1 \rightarrow E_g^0, \quad T_{2g}^2 \rightarrow E_g^1$$

For the first order strain derivatives $d_{\bar{\mathbf{q}}\mathbf{q}\beta}^{\alpha\alpha'}$, there will be six allowed terms at the Γ-point and 28 allowed at an X-point (see Table II and Ref. [51], equations S28 and S29). It should be noted that there is always one allowed identity strain derivative for each $d_{\bar{\mathbf{q}}\mathbf{q}}^{\alpha\alpha'}$, and the selection rules are more involved for non-identity strains. For the second order strain derivatives $d_{\bar{\mathbf{q}}\mathbf{q}\beta_1\beta_2}^{\alpha\alpha'}$, there will be 17 allowed terms at the Γ-point and 88 allowed terms at an X-point (see equations S30 and S31, and Table SIII in Ref. [51]). For the elastic energy, there are three $d_{\beta_1\beta_2}$, six $d_{\beta_1\beta_2\beta_3}$, and eleven $d_{\beta_1\beta_2\beta_3\beta_4}$ (see Table II and Ref. [51], Table SIII and Eq. S27). It should be noted that not all symmetry allowed terms will contribute to the finite temperature properties within the QHA unless there is a spontaneously broken symmetry. These 159 irreducible
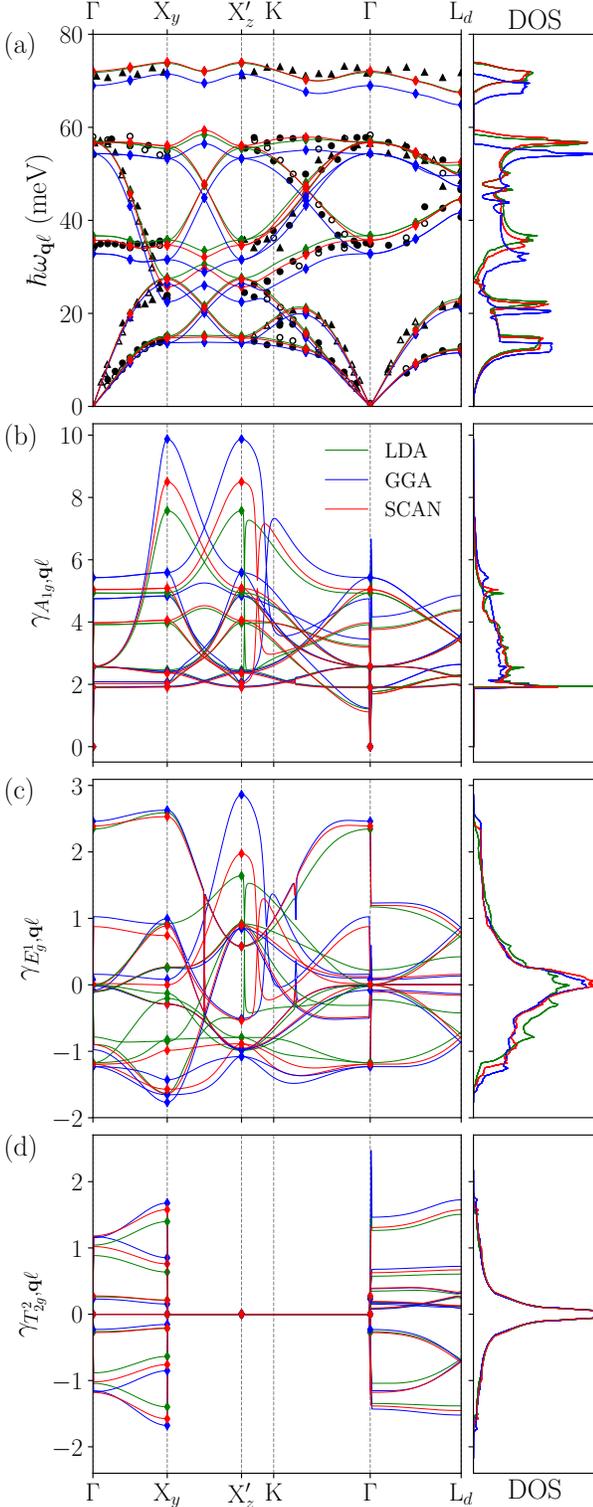
FIG. 1. The phonons and select Gruneisen parameters computed at $\hat{\mathbf{a}}_o$ using LDA, GGA, and SCAN. Each case contains a plot along high symmetry directions and the DOS (see Ref. [51], Table SI for definitions of $\mathbf{q}$). Diamonds are computed using DFT and corresponding lines are a Fourier interpolation. (a) The phonons are compared with experimental results (open markers [41] and closed markers [61]). (b, c, d) Generalized Gruneisen parameters.

ThO$_2$ Irreducible derivatives of $\mathcal{V}_{qh}$ for $\mathcal{N} \leq 3$							
(a) Elastic energy irreducible strain derivatives							
Derivative	LDA	GGA	SCAN	Derivative	LDA	GGA	SCAN
$d_{A_{1g}A_{1g}}$	170	158	166	$d_{E_g E_g}$	67.1	67.8	70.8
$d_{T_{2g}T_{2g}}$	23.0	19.9	22.5	$d_{A_{1g}A_{1g}A_{1g}}$	-955	-895	-938
$d_{A_{1g}E_g E_g}$	-108	-115	-116	$d_{A_{1g}T_{2g}T_{2g}}$	-180.	-185	-189
(b) $\Gamma-$point irreducible displacement and strain derivatives							
Derivative	LDA	GGA	SCAN	Derivative	LDA	GGA	SCAN
$d^{T_{2g}T_{2g}}_{\Gamma \; \Gamma}$	12.42	11.31	12.31	$d^{T_{2g}T_{2g}}_{\Gamma \; \Gamma \; A_{1g}}$	-63.4	-58.1	-63.4
$d^{T_{1u}T_{1u}}_{\Gamma \; \Gamma}$	13.58	10.87	12.88	$d^{T_{1u}T_{1u}}_{\Gamma \; \Gamma \; A_{1g}}$	-133.9	-118.0	-129.9
$d^{T_{2g}T_{2g}}_{\Gamma \; \Gamma \; E_g}$	-29.1	-27.8	-29.4	$d^{T_{2g}T_{2g}}_{\Gamma \; \Gamma \; T_{2g}}$	-6.5	-5.2	-6.8
$d^{T_{1u}T_{1u}}_{\Gamma \; \Gamma \; E_g}$	0.0	-1.7	0.2	$d^{T_{1u}T_{1u}}_{\Gamma \; \Gamma \; T_{2g}}$	-28.3	-25.1	-30.4
(c) X_z-point irreducible displacement and strain derivatives							
Derivative	LDA	GGA	SCAN	Derivative	LDA	GGA	SCAN
$d^{A_{1g}A_{1g}}_{X_z \; X_z}$	20.8	19.5	21.0	$d^{A_{1g}A_{1g}}_{X_z \; X_z \; A_{1g}}$	-80.3	-75.5	-79.8
$d^{E_g E_g}_{X_z X_z}$	4.90	3.81	4.60	$d^{E_g E_g}_{X_z X_z A_{1g}}$	-48.4	-42.6	-46.7
$d^{A_{2u}A_{2u}}_{X_z \; X_z}$	42.3	38.7	41.5	$d^{A_{2u}A_{2u}}_{X_z \; X_z \; A_{1g}}$	-176.1	-160.0	-168.1
$d^{B_{1u}B_{1u}}_{X_z \; X_z}$	2.91	1.93	2.53	$d^{B_{1u}B_{1u}}_{X_z \; X_z \; A_{1g}}$	-44.0	-38.2	-43.0
$d^{E_u E_u}_{X_z X_z}$	12.71	10.38	12.05	$d^{E_u E_u}_{X_z X_z A_{1g}}$	-111.3	-98.4	-105.3
$d^{E_u \, {}^1E_u}_{X_z X_z}$	-0.9	0.2	-0.7	$d^{E_u \, {}^1E_u}_{X_z X_z A_{1g}}$	71.8	63.1	69.5
$d^{{}^1E_u \, {}^1E_u}_{X_z \; X_z}$	11.77	10.87	12.02	$d^{{}^1E_u \, {}^1E_u}_{X_z \; X_z \; A_{1g}}$	-57.1	-52.5	-56.3
$d^{E_g E_g}_{X_z X_z B_{1g}}$	-5.9	-4.0	-4.7	$d^{E_g E_g}_{X_z X_z B_{2g}}$	13.7	12.8	14.5
$d^{E_u E_u}_{X_z X_z B_{1g}}$	-33.7	-32.4	-32.4	$d^{A_{2u}B_{1u}}_{X_z \; X_z \; B_{2g}}$	38.8	37.5	39.1
$d^{E_u \, {}^1E_u}_{X_z X_z \; B_{1g}}$	-6.2	-7.3	-7.4	$d^{E_u E_u}_{X_z X_z B_{2g}}$	-19.2	-17.1	-20.7
$d^{{}^1E_u \, {}^1E_u}_{X_z \; X_z \; B_{1g}}$	57.0	53.8	56.9	$d^{{}^1E_u E_u}_{X_z \; X_z B_{2g}}$	20.0	18.6	21.2
$d^{A_{1g}A_{1g}}_{X_z \; X_z \; {}^1A_{1g}}$	-23.9	-22.7	-24.3	$d^{{}^1E_u \, {}^1E_u}_{X_z \; X_z \; B_{2g}}$	-4.8	-3.4	-4.9
$d^{E_g E_g}_{X_z X_z {}^1A_{1g}}$	7.8	8.2	8.1	$d^{A_{1g}E_g}_{X_z \; X_z \; E_g}$	-22.5	-21.7	-23.2
$d^{A_{2u}A_{2u}}_{X_z \; X_z \; {}^1A_{1g}}$	44.2	39.3	44.5	$d^{A_{2u}E_u}_{X_z \; X_z \; E_g}$	-89.3	-82.8	-89.7
$d^{B_{1u}B_{1u}}_{X_z \; X_z \; {}^1A_{1g}}$	-9.5	-11.1	-10.0	$d^{A_{2u}\,{}^1E_u}_{X_z \; X_z \; E_g}$	32.0	28.6	31.7
$d^{E_u E_u}_{X_z X_z {}^1A_{1g}}$	-22.1	-18.0	-20.6	$d^{B_{1u}E_u}_{X_z \; X_z \; E_g}$	22.3	19.1	23.0
$d^{E_u \, {}^1E_u}_{X_z X_z \; {}^1A_{1g}}$	-8.4	-9.2	-9.2	$d^{B_{1u}\,{}^1E_u}_{X_z \; X_z \; E_g}$	-9.3	-8.5	-10.3
$d^{{}^1E_u \, {}^1E_u}_{X_z \; X_z \; {}^1A_{1g}}$	23.2	21.2	23.0				

TABLE II. Irreducible derivatives of $\mathcal{V}(\boldsymbol{\epsilon}, \mathbf{u})$ which parametrize the QHA for $\mathcal{N} \leq 3$ using $\hat{\mathbf{S}}_{BZ} = \hat{\mathbf{S}}_C$ (see Section III C 1 for definition of notation) evaluated at $\hat{\mathbf{a}}_o$. (a) Strain derivatives of $\mathcal{V}(\boldsymbol{\epsilon}, \mathbf{0})$ in units of eV. (b, c) Second displacement derivatives and corresponding strain derivatives in units of eV/Å^2.

derivatives completely specify Eq. 94 for $\mathcal{N} \leq 4$ at a resolution of $\hat{\mathbf{S}}_{BZ} = \hat{\mathbf{S}}_C$, and any observable can now be computed within the QHA under these assumptions. It is first useful to evaluate intermediate quantities which appear within the QHA equations, such as the strain derivatives of the phonon frequencies and the generalized Gruneisen parameters.

The irreducible derivatives $d^{\alpha\alpha'}_{\bar{\mathbf{q}}\mathbf{q}}$ and $d^{\alpha\alpha'}_{\bar{\mathbf{q}}\mathbf{q}\beta}$ are used to compute the generalized Gruneisen parameters $\gamma_{i,\mathbf{q}\ell}$ for each strain (see Eq. 70), and the $\gamma_{i,\mathbf{q}\ell}$ appear in equations 73 and 76. The A_{1g}, E_g^1, and T_{2g}^2 Gruneisen param-

eters evaluated at $\hat{\mathbf{a}}_o$ using LDA, GGA, and SCAN are shown in Figure 1 panels b, c, and d, respectively, with each corresponding Gruneisen DOS (see Supplementary Material, Figure S3 for the other three cases). While there are some noteworthy differences between the three DFT functionals, the resulting Gruneisen DOS are similar overall, consistent with the fact that $d_{\bar{\mathbf{q}}\mathbf{q}}^{\alpha\alpha'}$ and $d_{\bar{\mathbf{q}}\mathbf{q}\beta}^{\alpha\alpha'}$ are similar among the three functionals. For cubic systems, the A_{1g} Gruneisen parameter is proportional to the usual volumetric Gruneisen parameter $\gamma_{\mathbf{q}\ell}$, defined using a volumetric strain derivative (see Eq. 32), where $\gamma_{\mathbf{q}\ell} = \gamma_{A_{1g},\mathbf{q}\ell}/\sqrt{3}$. There is a noticeable swapping of two A_{1g} Gruneisen bands between the X_z and K points which is caused by phonon bands which transform like the same irreducible representation and have an avoided crossing (see Ref. [51], Section SII for a detailed discussion).

We now discuss the non-identity Gruneisen parameters, which use strains that break the symmetry of the point group of the crystal, and these are not typically presented in the literature. Non-identity strains yield nontrivial selection rules for determining irreducible strain derivatives of the phonons. In particular, the non-identity strains in ThO$_2$ transform like multidimensional irreducible representations, and we present the results of the selection rules in Supplementary Material [51]. The non-identity Gruneisen parameters must average to zero in order for the crystal to be stable in the classical limit. For the case of ThO$_2$, the non-identity Gruneisen DOS integrates to zero, as expected (see Figure 1 panels c, d, for example). While the E_g^1 Gruneisen parameter has nonzero values along the presented high symmetry path, the T_{2g}^2 Gruneisen are zero over a substantial portion of the path, which is required by group theory (see Ref. [51] section SII).

While the irreducible derivatives $d_{\bar{\mathbf{q}}\mathbf{q}}^{\alpha\alpha'}$ and $d_{\bar{\mathbf{q}}\mathbf{q}\beta}^{\alpha\alpha'}$ are similar among the three DFT functionals, there are notable differences in $d_{\bar{\mathbf{q}}\mathbf{q}\beta_1\beta_2}^{\alpha\alpha'}$ (see Ref. [51], Table SIII). It should be emphasized that the differences are not numerical artifacts (see Ref. [51] Figure S10). It is useful to examine the second strain derivative of the phonon frequencies to appreciate the differences in $d_{\bar{\mathbf{q}}\mathbf{q}\beta_1\beta_2}^{\alpha\alpha'}$ (see Figure 2). While there are relatively small differences between the LDA and GGA functionals, SCAN is notably different. Therefore, the quartic terms computed from the SCAN functional have nontrivial differences.

Having established both the strain grid interpolation and strain Taylor series parameterizations, we can now evaluate the QHA. If not stated, it is implied that a given QHA calculation is evaluated at zero stress. The first task is to establish how large of a supercell $\hat{\mathbf{S}}_{BZ}$ is needed in order to sufficiently converge the observables, and we use both the CLTE (see Eq. 36) and the identity strain elastic constant $C_{A_{1g}A_{1g}}^{\text{iso}}$ (see Eq. 45) as measures; where the QHA using an $\mathcal{N} \leq 4$ Taylor series is employed. There is no appreciable difference between $\hat{\mathbf{S}}_{BZ} = \hat{\mathbf{S}}_C, 2\hat{\mathbf{1}}, 2\hat{\mathbf{S}}_C, 4\hat{\mathbf{1}}$ up to $T = 1500K$ (see Figure 3). Therefore, $\hat{\mathbf{S}}_{BZ} = \hat{\mathbf{S}}_C$ is used for all subsequent calculations of thermal expansion and elastic constants. It
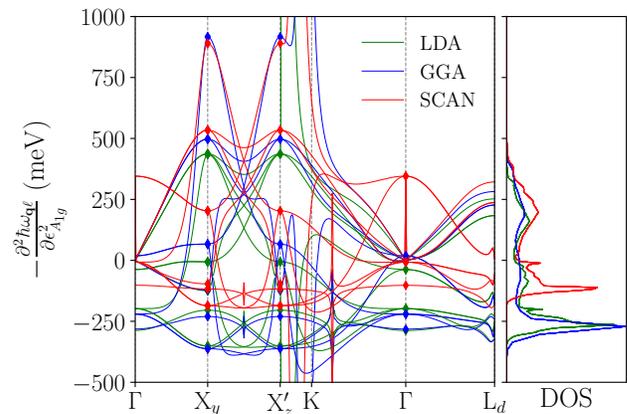
FIG. 2. The second A_{1g} strain derivative of the phonon frequencies evaluated at $\hat{\mathbf{a}}_o$ plotted along high symmetry directions for LDA, GGA, and SCAN; in addition to the DOS. Diamonds are computed using DFT and corresponding lines are a Fourier interpolation.

should be noted that the supercell convergence is not as rapid if LO-TO splitting is neglected (see Ref. [51], Figure S9 for a comparison). It is also possible to separately study the supercell convergence of the harmonic and anharmonic contributions (see Ref. [51] Figure S4).

Having established supercell convergence, we are now in a position to directly compare the strain grid interpolation and Taylor series parametrizations of the QHA; and we focus on the CLTE. Figure 4 shows how the $\mathcal{N} \leq 3$ and $\mathcal{N} \leq 4$ parametrizations reproduce the strain grid interpolation for the thermal expansion at increasingly high temperatures, respectively. The thermal expansion illustrates that, within the QHA, the quartic terms have an appreciable influence for $T \gtrsim 150$ K and terms beyond quartic have an appreciable influence for $T \gtrsim 1250$ K. Given that we will be comparing to experiments below $T = 1500$ K, it should be sufficient to employ $\mathcal{N} \leq 4$ in all comparisons with experiment. In addition to comparing the CLTE, it is interesting to compare the lattice parameter at $T = 0$, which includes zero point motion, among the three parametrizations. For the case of LDA, $\mathcal{N} \leq 3$, $\mathcal{N} \leq 4$, and the grid interpolation interpolation yield lattice parameters of 5.5415, 5.5413, and 5.5412 Å, respectively, yielding negligible differences. It is also interesting to explore the classical limit of the thermal expansion (see Figure 4, dotted lines), whereby $n_{\mathbf{q}\ell} \to k_B T/(\hbar\omega_{\mathbf{q}\ell})$ and the zero point motion is neglected. The leading order behavior of the classical thermal expansion is dictated by Eq. 89, which includes terms for $\mathcal{N} = 4$. Therefore, the $\mathcal{N} \leq 3$ and $\mathcal{N} \leq 4$ classical results have the same $T = 0K$ intercept, but the slope for $\mathcal{N} \leq 3$ is an approximation of the exact classical QHA slope due to $\ddot{\Omega}(\mathbf{0})$ lacking the quartic contribution. The q-averaged A_{1g} Gruneisen parameter $-\dot{\Omega}(\mathbf{0})$ (see Eq. 86) is 29.7, 32.2, and 29.9 for LDA, GGA, and SCAN respectively. The values of $\ddot{\Omega}(\mathbf{0})$ are -127.7, -164.5, and -169.1 for LDA, GGA, and SCAN,
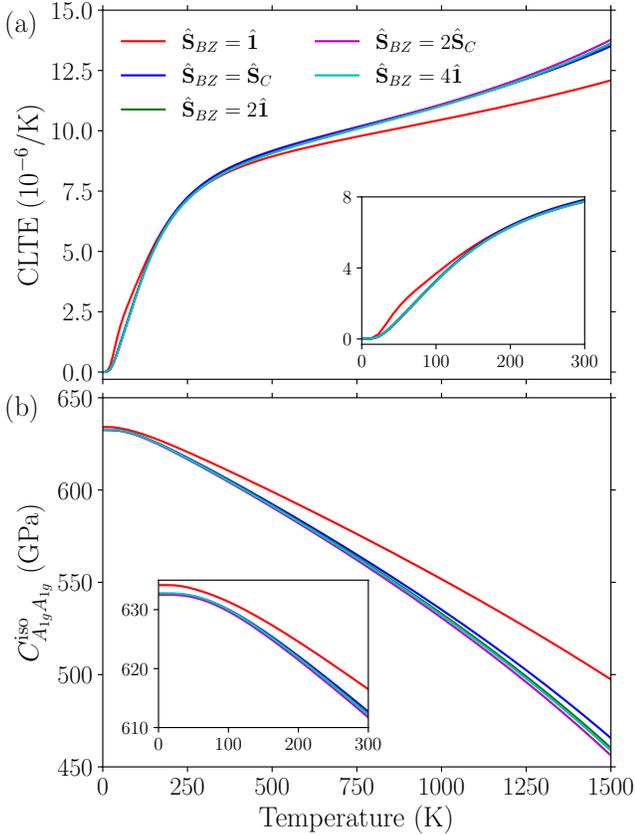
FIG. 3. The coefficient of linear thermal expansion (CLTE, panel a) and identity strain elastic constant $C^{\mathrm{iso}}_{A_{1g}A_{1g}}$ (panel b) as a function of temperature for increasing supercell sizes (i.e. $\hat{\mathbf{S}}_{BZ}$) computed using QHA (LDA, $\mathcal{N} \leq 4$). The insets focus on the low temperature regime. A Fourier interpolation mesh of $10\hat{\mathbf{1}}$ was used in all cases.
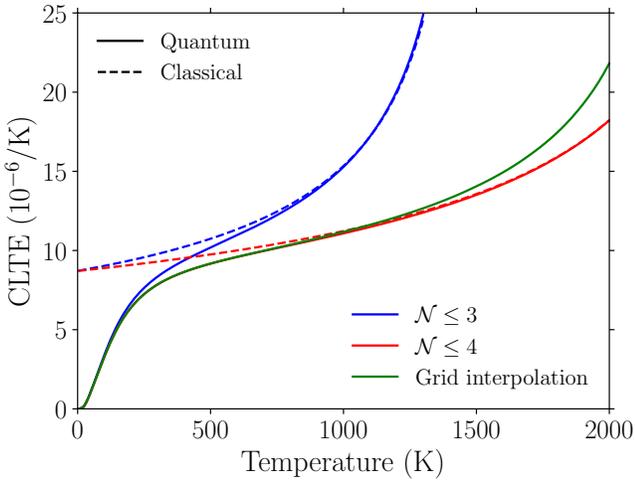
FIG. 4. The coefficient of linear thermal expansion as a function of temperature for the strain grid interpolation and Taylor series parameterizations of $\mathcal{V}_{qh}$ (using LDA). The classical results are shown as dotted lines.

Method (0 K)	a	C^{adi}_{11}	C^{adi}_{12}	C^{adi}_{44}
LDA	5.541	376.3	127.6	85.0
	5.496[a]	390[a,iso]	125[a,iso]	93[a,iso]
PBEsol	5.53[a]	373.3[a,iso]	114.6[a,iso]	83.4[a,iso]
GGA	5.632	345.3	106.3	70.2
SCAN	5.603	367.3	114.3	79.7
Method (300 K)	a	C^{adi}_{11}	C^{adi}_{12}	C^{adi}_{44}
LDA	5.549	368.7	125.0	82.4
	5.503[a]	385.7[a,iso]	122.5[a,iso]	90.4[a,iso]
PBEsol	5.545[a]	368.8[a,iso]	112.3[a,iso]	80.7[a,iso]
GGA	5.642	336.1	102.9	67.2
SCAN	5.611	358.5	111.1	76.3
Expt.	5.600[c]	377[g,iso]	146[g,iso]	89[g,iso]
	5.662[b]	367[e]	106[e]	79.7[e]
	5.597[f]	-	-	-
XRD	5.5989	-	-	-

[iso] Isothermal elastic constant

[a] Ref. [32], [b] Ref. [37], [c] Ref. [82], [d] Ref. [83], [e] Ref. [42], [f] Ref. [84], [g] Ref. [41]

TABLE III. The QHA calculated lattice parameter in units of Å and elastic constants in units of GPa, in addition to experimental values and previous calculations at $T = 0$ K and at $T = 300$ K.

respectively. The values of $\ddot{\mathcal{V}}(\mathbf{0})$ and $\dddot{\mathcal{V}}(\mathbf{0})$ are given in Table II.

We now proceed to present our results for thermal expansion and compare to experiments. We begin by analyzing the lattice constant as a function of temperature (see Figure 5, panel a). Most of the experimental results (points and dotted line) are in relatively good agreement, with the exception of the data from Wachtman $et.$ al[37], which are mainly offset to higher lattice parameters by a constant. The dotted line in panel a is a quadratic fit to various experimental results, parameterized by Taylor [39]. Our X-ray diffraction result on the sample at $T = 300$ K is in good agreement with the experimental consensus. The neutron scattering results from HYSPEC also contain elastic scattering, including 4 Bragg peaks, which have been measured from $T = 300$ K to $T = 1200$ K. The instrument is not optimized to measure elastic scattering to high precision and the lattice parameter results are not as precise as conventional XRD or other comparable methods. However, the errors may not depend strongly on temperature, and therefore we shift all lattice parameters extracted from neutron scattering by a constant (i.e., $+0.883$ pm) such that the results for $T = 300$ K match our XRD results. This brings the neutron scattering lattice parameter results into agreement with previously reported values. The QHA results within LDA, GGA, and SCAN (solid lines) demonstrate that SCAN has the best agreement with experiment, and the largest difference over the plotted temperature range

is only approximately half of a percent. As might be expected, the LDA result consistently underpredicts the lattice parameter, while GGA overpredicts.

We now compare our QHA CLTE results to previous experiments (see Figure 5, panel b). The experimental results are all within reasonable agreement, and the discontinuity in Taylor's parameterization is due to there being three temperature regimes where the fit is performed. Within the QHA, LDA agrees best with experimental results, SCAN predicts a slightly larger expansion, and GGA predicts the largest thermal expansion. However, the QHA is a truncation of the vibrational Hamiltonian, and therefore the functional with the best QHA computed observables as compared with experiment might not be delivering the most accurate solution as compared to the exact solution of the many-phonon problem. Going beyond the QHA, which implies solving a $\mathcal{V}$ that includes third order and higher displacements derivatives which are not present in $\mathcal{V}_{qh}$, could be expected to have an opposing effect on the temperature dependence of the thermal expansion with a similar magnitude [3]. In the ionic insulators MgO and NaCl, including third and fourth order displacement derivatives and using the self-consistent phonon method decreases the CLTE as compared to the QHA [85]. Therefore, it seems likely that LDA may not yield the best CLTE when a higher level of theory is used. The nonlinear behavior of the CLTE above $T = 1000$ K for GGA and SCAN has been seen in numerous QHA calculations of ionic insulators in the literature, such as MgO [8], Al_2O_3 [13], and $MgSiO_3$ [24]. Our LDA QHA results are similar to previous publications using LDA [30, 32], though there are some differences (see Ref. [51]). For convenience, the $T = 0$ K and $T = 300$ K results from theory and experiment are compiled in Table III.

Having computed $\tilde{\epsilon}(T, \mathbf{0})$, the phonon dispersion can now be evaluated at an arbitrary temperature within the QHA. The phonons computed with SCAN using $\hat{\mathbf{S}}_{BZ} = 4\hat{\mathbf{1}}$ within the $\mathcal{N} \leq 4$ Taylor series is shown for temperatures of $T = 5$ K, $T = 300$ K, and $T = 750$ K (see Figure 6, solid lines and points). The differences in our predicted values between $T = 5$ K and $T = 300$ K are extremely small, given the small change in the lattice parameter over this temperature range (see Figure 5, panel a). Alternatively, the differences between $T = 300$ K and $T = 750$ K are non-negligible, with a change as large as 1.5 meV, which is expected given the larger change in the lattice parameter. We also present INS measurements at the respective temperatures (hollow points). The general trend of the INS results is a softening of the phonons with increasing temperature, consistent with the QHA, but the resolution of INS makes it challenging to quantitatively assess the performance of the QHA results.

We now consider the elastic constants (Eq. 44) at zero temperature, which have two zero point contributions: one from the zero point identity strain and the other directly from the strain derivative of the zero point free energy. It is useful to illustrate the magnitude of these zero point contributions, and we take C_{11} com-
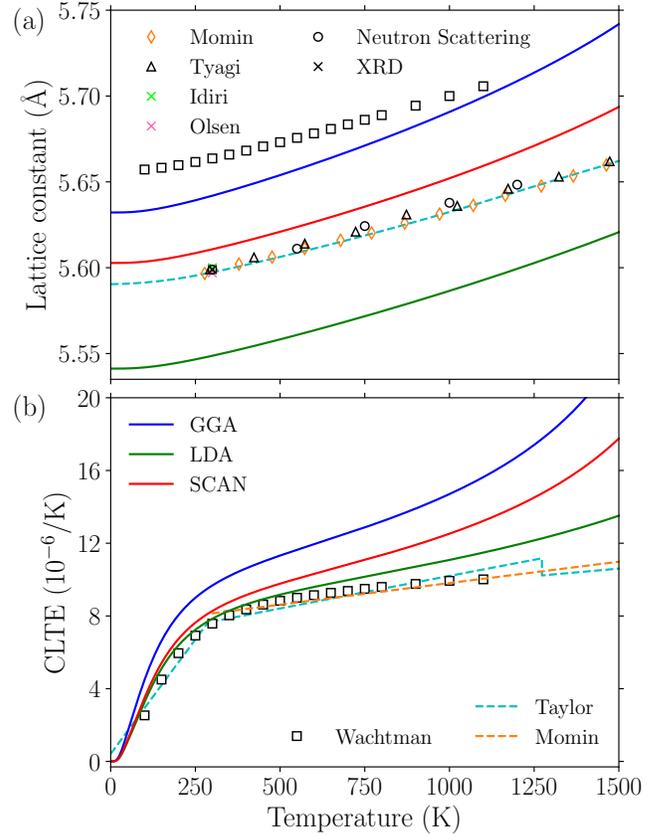
FIG. 5. The lattice parameter and coefficient of linear thermal expansion computed within QHA ($\mathcal{N} \leq 4$) using LDA, GGA, and SCAN (solid lines) in addition to experimental results. (a) The lattice parameter: QHA (solid lines), our XRD (black x) and neutron scattering measurements (circle), and previous experimental results[37–39, 82, 84, 86]. (b) The coefficient of linear thermal expansion: QHA (solid lines) and previous experimental results[37–39].

puted at $T = 0$ using SCAN as an example. The classical value of C_{11} can be obtained using results from Tables I and II as $4(d_{A_{1g}A_{1g}} + 2d_{E_gE_g})/(3a_o^3) = 375.8$ GPa, where $a_o^3/4$ is the classical volume of the primitive unit cell at $T = 0$. The zero point identity strain, which is the strain defined relative to the classical lattice at zero temperature due to quantum fluctuations, has a value of $\tilde{\epsilon}_{A_{1g}}(0, \mathbf{0}) = 3.25 \times 10^{-3}$. The zero point identity strain renormalizes the volume to $a_o^3(1 + \tilde{\epsilon}_{A_{1g}}(0, \mathbf{0})/\sqrt{3})^3/4$, activates higher order terms from Tables II and SIII, and changes the reference frame according to Eq. 14 and Eq. 20, resulting in the following addition to the classical elastic constant,

$$\frac{4}{3a_o^3(1 + \epsilon_{A_{1g}}/\sqrt{3})}\Big((d_{A_{1g}A_{1g}A_{1g}} + 2d_{E_gE_gA_{1g}})\epsilon_{A_{1g}} + \frac{1}{2}(d_{A_{1g}A_{1g}A_{1g}A_{1g}} + 2d_{E_gE_gA_{1g}A_{1g}})\epsilon_{A_{1g}}^2\Big), \qquad (99)$$

and shifts C_{11} to 370.5 GPa. The contribution from the
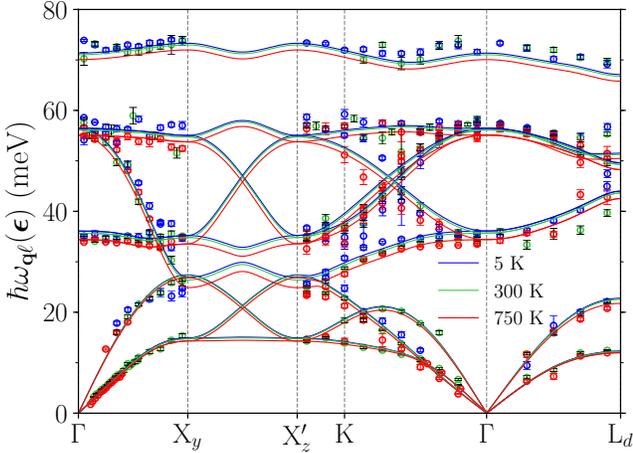
FIG. 6. The phonons computed within the QHA ($\mathcal{N} \leq 4$) using SCAN (solid points and lines) and inelastic neutron scattering measurements (hollow points) at $T = 5, 300, 750$ K along high symmetry directions. The same color scheme is used for QHA and INS.

second order derivative of the zero point free energy with respect to ϵ_1, will result in

$$\frac{\hbar}{Na_o^3(1 + \epsilon_{A_{1g}}/\sqrt{3})} \sum_{\mathbf{q}\ell} \frac{\partial^2 \omega_{\mathbf{q}\ell}(\boldsymbol{\epsilon})}{\partial \epsilon_1^2}\bigg|_{\tilde{\epsilon}_{A_{1g}}}, \qquad (100)$$

evaluating to -3.3 GPa, and finally yielding a C_{11} of 367.2 GPa; which is 0.1 GPa lower than the value reported in Table III due to the precision in which the irreducible derivatives are reported in Table II. Thus we see that zero point motion introduces a 1.4 percent decrease in C_{11} due to the zero point identity strain and a further 0.9 percent due to the second strain derivative of the vibrational free energy. It should be noted that the quasistatic approximation to the QHA only retains the first contribution (see Ref. [51], Section SIII for further comparison).

The temperature dependent elastic constants can now be presented in either the symmetrized or the standard basis, and we opt for the latter. We compute the adiabatic and isothermal C_{11}, C_{12}, and C_{44} using LDA, GGA, and SCAN within QHA for $\mathcal{N} \leq 4$ (see Figure 7, panels a, b, c, respectively). In all cases, LDA, SCAN, and GGA produce successively smaller elastic constants. The different DFT functionals produce some notable differences in the temperature dependence of the elastic constants, which is to be expected given some of the appreciable differences in the quartic terms (recall the discussion surrounding Figure 2). For example, C_{44} within SCAN decreases notably faster than within LDA and GGA (see Ref. [51] Sec. SIII for a discussion). At high temperatures, the softening predicted by the QHA is rather dramatic, which should be treated with caution given the simplicity of the QHA. For example, we previously argued that going beyond the QHA might decrease the predicted value of the thermal expansion, which would
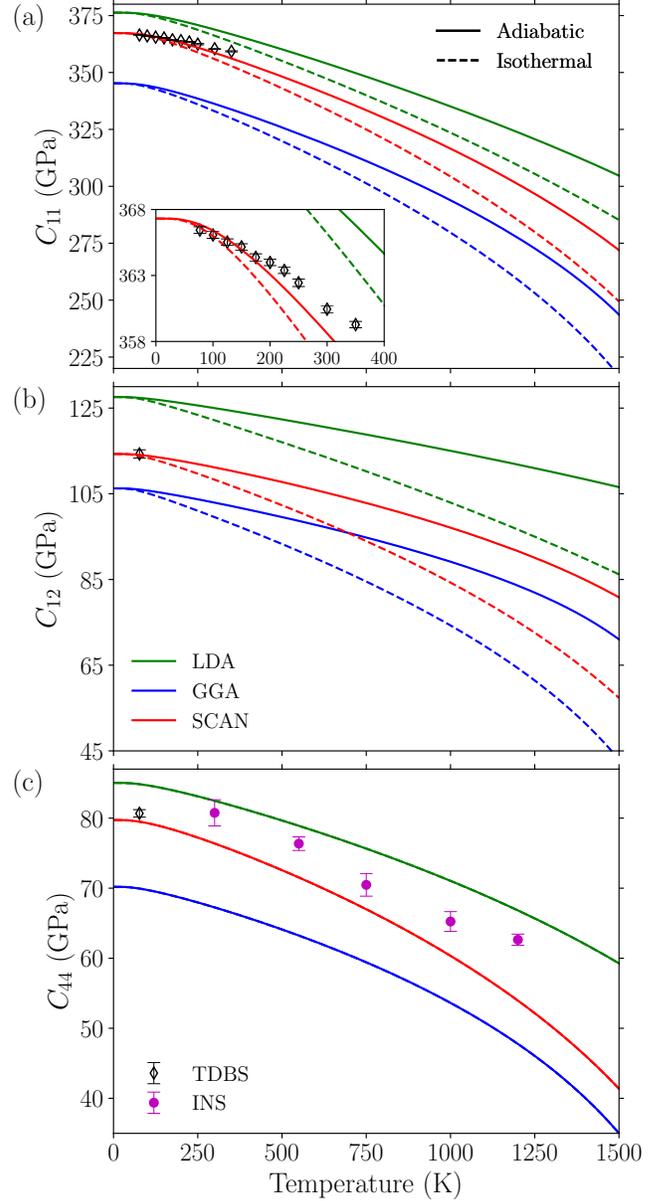
FIG. 7. The elastic constants C_{11}, C_{12}, C_{44} (panels a,b, and c, respectively) computed using QHA ($\mathcal{N} \leq 4$) with LDA, GGA, and SCAN and our TDBS (diamonds) and INS (circles) measurements. Open markers and solid lines denote adiabatic conditions whereas dashed lines and closed markers denote isothermal conditions. For C_{44}, adiabatic and isothermal conditions yield the same results.

then diminish the predicted softening of the elastic constants.

We now compare to our experimental measurements of the elastic constants. The TDBS results correspond to adiabatic conditions, and use the temperature-dependent experimental volume from the fit in Ref. [39]. For the lowest temperature probed in TDBS, $T = 77$ K, the QHA dictates that the anharmonicity only has a minimal effect, demonstrating that the SCAN functional

overwhelmingly has the best agreement with experiment in the harmonic regime. The largest difference in the $T = 77$ K experiment and SCAN functional results is -1.7 percent for C_{44}, while both LDA and GGA have nontrivial errors. Considering the temperature dependence of TDBS for C_{11}, the SCAN functional has the best agreement in terms of the absolute value, but decreases too quickly with temperature. For the INS measurements of C_{44}, the results are roughly between the SCAN and LDA results. As discussed previously, using a theory which is more sophisticated than the QHA may diminish the predicted softening, which would bring the SCAN results closer to experiment.

Having evaluated the temperature dependence of various observables under zero stress conditions, we now explore the pressure dependence of the bulk modulus at $T = 300$ K to leading order in pressure using Eq. 54 and Eq. 52 with the $\mathcal{N} \leq 4$ Taylor series (see Fig. 8). Our results are compared to two previous experimental results [82, 84] which have zero pressure intercepts of 198 and 195 GPa, respectively, and slopes at zero pressure of 4.6 and 5.4, respectively; putting the two experimental results in reasonable agreement. We begin by analyzing the zero pressure result, which is already contained within our previous analysis of C_{11} and C_{12} at $T = 300$ K and zero pressure. For C_{11}, GGA substantially underestimated, LDA substantially overestimated, and SCAN mildly underestimated the TDBS results; and similar conclusions held for C_{12} at $T = 77$ K. Therefore, we expect the same trend to hold for the bulk modulus at $T = 300$ K, which suggests that the result of Olsen *et al.* might be more consistent with TDBS; and is closer to the result of Macedo *et al.* [42]. The three DFT functionals all produce comparable slopes, which are closer in value to the slope of Idiri *et al.*

VII. CONCLUSIONS

Here we presented the most general version of the QHA, allowing for the computation of observables at a given temperature and true stress in an arbitrary crystal; implemented purely using space group irreducible derivatives. We cast the generalized QHA in terms of a truncation of the Born-Oppenheimer potential, retaining the strain dependence of the elastic energy and the dynamical matrix. The resulting vibrational Hamiltonian is therefore quadratic and the quantum partition function can be written in closed form in terms of the phonon frequencies, allowing for a straightforward numerical evaluation of the Helmholtz free energy as a function of strain. The strain map can then be constructed as a function of temperature and true stress via inversion, allowing for the evaluation of thermodynamic observables at constant temperature and true stress. It should be noted that the general formalism that we presented for evaluating observables at constant temperature and true stress is written in terms of the exact free energy, and therefore can be used with
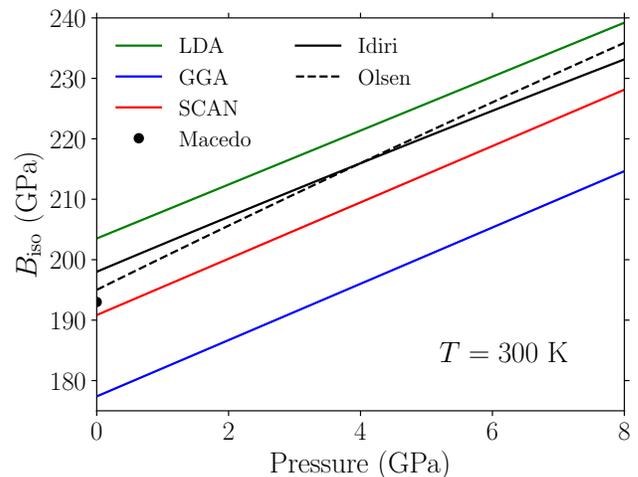
FIG. 8. The isothermal bulk modulus as a function of pressure at $T = 300$ K. The experimental curves were extracted from the published equations of state[82, 84]; the zero pressure result is from Ref. [42]. The theoretical results were computed using the QHA with $\mathcal{N} \leq 4$ to leading order in pressure for LDA, GGA, and SCAN.

approximations that go beyond the generalized QHA.

A key feature of our approach to the generalized QHA is that the dynamical matrix is always resolved in terms of space group irreducible displacement derivatives, guaranteeing that our vibrational Hamiltonian satisfies symmetry by construction. All irreducible derivatives are computed using the lone irreducible derivative (LID) approach, which individually computes each irreducible derivative using central finite difference in the smallest supercell allowed by group theory. Executing the QHA requires the parametrization of the strain dependence of two key quantities: the elastic energy and the irreducible second order displacement derivatives. We explore two complementary approaches for executing the parametrization: a Taylor series expansion in terms of the irreducible representations of strain and a grid of strains which is then interpolated. The first approach is beneficial in that the QHA is guaranteed to be correct order by order, while the latter will yield reasonable QHA results even in the case of large strains and temperatures.

The generalized QHA is illustrated in the case of ThO_2 using the LDA, GGA, and SCAN approximations for the DFT exchange-correlation functional. We compute the temperature dependence of the thermal expansion and the full elastic constant tensor, in addition to the pressure dependence of the bulk modulus at $T = 300$ K. Special attention is devoted to studying the range convergence of the thermal expansion and identity strain elastic constant, demonstrating that reasonable convergence is already obtained using irreducible derivatives from the conventional cubic supercell. We demonstrate that a quartic Taylor series and a grid interpolation of strain dependence within the QHA deliver comparable results

for thermal expansion up to approximately $T = 1200$ K. Within the strain Taylor series, the cubic terms are similar among the three DFT functionals, as are the quadratic terms, while the quartic terms can be drastically different for SCAN; which results in clear differences in computed observables.

In addition to comparing with previous experiments, we perform our own measurements of the elastic constants using time domain Brillouin scattering for $T = 77 - 350$ K and using inelastic neutron scattering for $T = 300 - 1200$ K. The SCAN functional delivers the most accurate prediction of the experimental lattice parameter up to the highest temperature evaluated, with an overprediction that is always less than 0.6 percent. For the coefficient of thermal expansion, all three functionals overpredict experiment, with LDA being slightly closer to experiment than SCAN. However, some degree of overprediction is anticipated due to the limitations of QHA. Our experimental measurements of the elastic constants at $T = 77$ K are in best agreement with the SCAN functional, with the largest error being 1.7%. SCAN predicts a temperature dependence for C_{44} which decreases more rapidly than measurements obtained from neutron scattering, though the discrepancy may be reasonable given the limitations of the QHA. The leading order pressure dependence of the bulk modulus at $T = 300$ K within the QHA is compared to experiment, showing reasonable agreement.

Our approach to the generalized QHA via irreducible derivatives greatly facilitates the implementation without further approximations and reduces the computational cost. Using only space group irreducible derivatives to parameterize the generalized QHA means that only a minimum amount of information is required, which facilitates dissemination of results, reproducibility, and high throughput applications. Furthermore, the generalized QHA can be viewed as a truncation to the Born-Oppenheimer potential, and therefore it is a natural starting point for more advanced approaches. Future work will directly include anharmonic displacement derivatives, and the resulting vibrational Hamiltonian will then be solved using a variety of techniques, including variational theories, classical molecular dynamics, and other approaches.

VIII. ACKNOWLEDGEMENTS

Appendix A: Non-analytic correction for ionic insulators

Ionic insulators require special treatment for the Fourier interpolation of phonons in order to correctly recover the polar phonon branches in the vicinity of the Γ-point, and we employ the standard dipole-dipole approach [81, 87]; which is normally used in conjunction with density functional perturbation theory[79]. While the standard dipole-dipole approach has been implied to be challenging to implement within finite displacement approaches for computing phonons[88], there is no difference between the implementation within finite displacement and perturbative approaches; though this may not be totally apparent. Indeed, others have reported calculations using the standard dipole-dipole approach in conjunction with finite displacement approaches[89], though no detailed description of their algorithm was provided. A brief outline of the standard dipole-dipole approach to polar insulators is given here using our notation and conventions for clarity, and it should be emphasized that our discussion is general to perturbative and finite displacement approaches to computing phonons.

First-principles approaches may be used to compute $D_{\mathbf{q}}^{ij}$ (see Eq. 63) in polar insulators over some discrete grid of $\mathbf{q}$-points defined by a finite translation group, which is dictated by some supercell. Strictly speaking, no correction is needed to account for electric fields due to polarization, as these effects are already accounted for in $D_{\mathbf{q}}^{ij}$. However, the polar branches are not well defined at the Γ-point, and can only be characterized in the limit of $\mathbf{q} \to \mathbf{0}$. Therefore, $D_{\mathbf{q}}^{ij}$ requires a special correction when interpolating, which can be achieved using the standard dipole-dipole approach.

We begin by recalling the standard Fourier interpolation algorithm (see [56] for notation and a detailed discussion). In this appendix, we will employ Cartesian reciprocal lattice points $\mathbf{Q}$, where $\mathbf{Q} = \mathbf{q}\hat{\mathbf{b}}$, and Cartesian real space lattice vectors $\mathbf{T}$, as opposed to lattice coordinates which are used throughout the manuscript. Fourier interpolation consists of four main steps. First, a set of $\hat{\mathbf{D}}_{\mathbf{Q}}$ are computed, where $\mathbf{Q} \in \tilde{Q}_{BZ}$ and $\tilde{Q}_{BZ} = \{\mathbf{q}\hat{\mathbf{b}} \,|\, \mathbf{q} \in$

$\tilde{q}_{BZ}$}. Second, the $\hat{\mathbf{D}}_{\mathbf{Q}}$ are Fourier transformed

$$\hat{\boldsymbol{\Phi}}_{\mathbf{T}} = \frac{1}{N} \sum_{\mathbf{Q} \in \tilde{Q}_{BZ}} e^{-i\mathbf{Q}\cdot\mathbf{T}} \hat{\mathbf{D}}_{\mathbf{Q}}. \tag{A1}$$

Third, Wigner-Seitz packing is performed

$$\{\hat{\boldsymbol{\Phi}}_{\mathbf{T}} \,|\, \mathbf{T} \in \tilde{T}_{BZ}\} \rightarrow \{\hat{\boldsymbol{\Phi}}_{\mathbf{T}}^{WS} \,|\, \mathbf{T} \in \tilde{T}_{BZ}^{WS}\}, \tag{A2}$$

where $\tilde{T}_{BZ} = \{\mathbf{t}\hat{\mathbf{a}} \,|\, \mathbf{t} \in \tilde{t}_{BZ}\}$ and $\tilde{T}_{BZ}^{WS} = \{\mathbf{t}\hat{\mathbf{a}} \,|\, \mathbf{t} \in \tilde{t}_{BZ}^{WS}\}$. Finally, the dynamical matrix can be predicted at an arbitrary $\mathbf{Q}$-point as

$$\hat{\mathbf{D}}_{\mathbf{Q}}^{FI} = \sum_{\mathbf{T} \in \tilde{T}_{BZ}^{WS}} e^{i\mathbf{Q}\cdot\mathbf{T}} \hat{\boldsymbol{\Phi}}_{\mathbf{T}}^{WS}, \tag{A3}$$

where the superscript FI differentiates the interpolated dynamical matrix from that over the discrete grid of $\mathbf{Q}$-points. It should be emphasized that $\hat{\mathbf{D}}_{\mathbf{Q}}^{FI} = \hat{\mathbf{D}}_{\mathbf{Q}}$ when $\mathbf{Q} \in \tilde{Q}_{BZ}$.

While $\hat{\mathbf{D}}_{\mathbf{Q}}^{FI}$ will interpolate $\hat{\mathbf{D}}_{\mathbf{Q}}$ to an arbitrary $\mathbf{Q}$-point, it will not properly interpolate the effects of the dipole-dipole interaction near the Γ-point. To remedy this deficiency, an analytic correction based on the dipole-dipole term can be directly added to $\hat{\mathbf{D}}_{\mathbf{Q}}^{FI}$, yielding the final interpolated dynamical matrix as

$$\hat{\mathbf{D}}_{\mathbf{Q}}^{FI} + \hat{\boldsymbol{\mathcal{D}}}_{\mathbf{Q}} - \hat{\boldsymbol{\mathcal{D}}}_{\mathbf{Q}}^{FI}, \tag{A4}$$

where the dipole-dipole contribution $\hat{\boldsymbol{\mathcal{D}}}_{\mathbf{Q}}$ is defined by [81],

$$\mathcal{D}_{\mathbf{Q}}^{\kappa\alpha,\kappa'\beta} = \widetilde{\mathcal{D}}_{\mathbf{Q}}^{\kappa\alpha,\kappa'\beta} - \delta_{\kappa\kappa'} \sum_{\kappa''} \widetilde{\mathcal{D}}_{\mathbf{Q}=\mathbf{0}}^{\kappa\alpha,\kappa''\beta}, \tag{A5}$$

where κ, κ' label atoms within the primitive cell, α, β label the displacement polarizations (i.e. x, y, and z directions), and

$$\widetilde{\mathcal{D}}_{\mathbf{Q}}^{\kappa\alpha,\kappa'\beta} = \sum_{\alpha'\beta'} Z_{\kappa,\alpha'\alpha}^* Z_{\kappa',\beta'\beta}^* \bar{\mathcal{D}}_{\mathbf{Q}}^{\kappa\alpha',\kappa'\beta'}, \tag{A6}$$

where $Z_{\kappa,\alpha'\alpha}^*$ is the Born effective charge and

$$\bar{\mathcal{D}}_{\mathbf{Q}}^{\kappa\alpha,\kappa'\beta} = \frac{4\pi}{|\hat{\mathbf{a}}|}$$
$$\begin{cases} \sum_{\mathbf{G}} \dfrac{(\mathbf{G}+\mathbf{Q})_\alpha (\mathbf{G}+\mathbf{Q})_\beta e^{i(\mathbf{G}+\mathbf{Q})\cdot(\mathbf{A}_\kappa - \mathbf{A}_{\kappa'})}}{\sum_{\gamma\gamma'} (\mathbf{G}+\mathbf{Q})_\gamma \epsilon_{\gamma\gamma'}^\infty (\mathbf{G}+\mathbf{Q})_{\gamma'}}, |\mathbf{Q}| > 0 \\[2ex] \sum_{\mathbf{G}\neq\mathbf{0}} \dfrac{G_\alpha G_\beta}{\sum_{\gamma\gamma'} G_\gamma \epsilon_{\gamma\gamma'}^\infty G_{\gamma'}} e^{i\mathbf{G}\cdot(\mathbf{A}_\kappa - \mathbf{A}_{\kappa'})}, \quad \mathbf{Q} = \mathbf{0} \end{cases}$$
$$\tag{A7}$$

where $\mathbf{G}$ is a Cartesian reciprocal lattice vector, $\mathbf{A}_\kappa$ is the Cartesian position of atom κ within the primitive unit cell, and $\epsilon_{\gamma\gamma'}^\infty$ is the dielectric tensor. Having defined $\hat{\boldsymbol{\mathcal{D}}}_{\mathbf{Q}}$, the Fourier interpolated counterpart $\hat{\boldsymbol{\mathcal{D}}}_{\mathbf{Q}}^{FI}$ can be obtained using the Fourier interpolation scheme outlined

in equations A1-A3, which completely defines the dipole-dipole interpolation algorithm. It should be emphasized that the $\mathbf{Q} = \mathbf{0}$ case of Eq. A7 will be utilized in the construction of $\hat{\boldsymbol{\mathcal{D}}}_{\mathbf{Q}}^{FI}$, and therefore $\hat{\boldsymbol{\mathcal{D}}}_{\mathbf{Q}=\mathbf{0}}^{FI}$ recovers the $\mathbf{Q} = \mathbf{0}$ case of Eq. A7. In the small $\mathbf{Q}$ limit, we have

$$\lim_{\mathbf{Q}\to\mathbf{0}} \left(\mathcal{D}_{\mathbf{Q}}^{\kappa\alpha,\kappa'\beta} - \mathcal{D}_{\mathbf{Q}}^{FI,\kappa\alpha,\kappa'\beta} \right) =$$
$$\frac{4\pi}{|\hat{\mathbf{a}}|} \frac{(\sum_\gamma \underline{Q}_\gamma Z_{\kappa,\gamma\alpha}^*)(\sum_{\gamma'} \underline{Q}_{\gamma'} Z_{\kappa',\gamma'\beta}^*)}{\sum_{\gamma\gamma'} \underline{Q}_\gamma \epsilon_{\gamma\gamma'}^\infty \underline{Q}_{\gamma'}} \tag{A8}$$

where $\underline{Q} = \mathbf{Q}/|\mathbf{Q}|$. Additionally, we have

$$\hat{\boldsymbol{\mathcal{D}}}_{\mathbf{Q}} = \hat{\boldsymbol{\mathcal{D}}}_{\mathbf{Q}}^{FI} \quad, \quad \mathbf{Q} \in \tilde{Q}_{BZ}, \tag{A9}$$

such that $\hat{\boldsymbol{\mathcal{D}}}_{\mathbf{Q}} - \hat{\boldsymbol{\mathcal{D}}}_{\mathbf{Q}}^{FI}$ cancels for all $\mathbf{Q} \in \tilde{Q}_{BZ}$. The above properties illustrate why $\hat{\boldsymbol{\mathcal{D}}}_{\mathbf{Q}} - \hat{\boldsymbol{\mathcal{D}}}_{\mathbf{Q}}^{FI}$ is the correction that may be added to $\hat{\mathbf{D}}_{\mathbf{Q}}$ in order to properly interpolate dipole-dipole effects.

The matrix elements $\bar{\mathcal{D}}_{\mathbf{Q}}^{\kappa\alpha,\kappa'\beta}$ are evaluated using the Ewald summation technique, where the $|\mathbf{Q}| > 0$ case in equation A7 can be evaluated as

$$\bar{\mathcal{D}}_{\mathbf{Q}}^{\kappa\alpha,\kappa'\beta} = \sum_{\mathbf{G} \text{ with } \mathbf{K}=\mathbf{G}+\mathbf{Q}} \frac{4\pi}{|\hat{\mathbf{a}}|} \frac{K_\alpha K_\beta}{\sum_{\gamma\gamma'} K_\gamma \epsilon_{\gamma\gamma'}^\infty K_{\gamma'}}$$
$$e^{i\mathbf{K}\cdot(\mathbf{A}_\kappa - \mathbf{A}_{\kappa'})} \exp\left(-\frac{\sum_{\gamma\gamma'} K_\gamma \epsilon_{\gamma\gamma'}^\infty K_{\gamma'}}{4\Lambda^2} \right)$$
$$- \sum_{\mathbf{T}} \Lambda^3 e^{i\mathbf{Q}\cdot\mathbf{T}} \frac{H_{\alpha,\beta}(\Lambda\boldsymbol{\Delta}_{\mathbf{T}\kappa\kappa'}, \Lambda D_{\mathbf{T}\kappa\kappa'})}{\sqrt{\det(\hat{\boldsymbol{\epsilon}}^\infty)}}$$
$$- \delta_{\kappa\kappa'} \frac{4\Lambda^3}{3\sqrt{\pi \det(\hat{\boldsymbol{\epsilon}}^\infty)}} ((\hat{\boldsymbol{\epsilon}}^\infty)^{-1})_{\alpha\beta}, \quad |\mathbf{Q}| > 0 \tag{A10}$$

where Λ is a damping term that is chosen such that each sum converges rapidly; the terms in the real space sum are defined as

$$\mathbf{d}_{\mathbf{T}\kappa\kappa'} = \mathbf{T} + \mathbf{A}_\kappa - \mathbf{A}_{\kappa'}, \tag{A11}$$

$$(\Delta_{\mathbf{T}\kappa\kappa'})_\alpha = \sum_\beta ((\epsilon^\infty)^{-1})_{\alpha\beta} (d_{\mathbf{T}\kappa\kappa'})_\beta, \tag{A12}$$

$$D_{\mathbf{T}\kappa\kappa'} = \sqrt{\Delta_{\mathbf{T}\kappa\kappa'} \cdot \mathbf{d}_{\mathbf{T}\kappa\kappa'}}, \tag{A13}$$

and

$$H_{\alpha,\beta}(\mathbf{x},y) = \frac{x_\alpha x_\beta}{y^2} \left[\frac{3}{y^3}\text{erfc}(y) + \frac{2}{\sqrt{\pi}} e^{-y^2}(\frac{3}{y^2}+2) \right]$$
$$- ((\epsilon^\infty)^{-1})_{\alpha\beta} \left[\frac{\text{erfc}(y)}{y^3} + \frac{2}{\sqrt{\pi}} \frac{e^{-y^2}}{y^2} \right]. \tag{A14}$$

The $\mathbf{Q} = \mathbf{0}$ case of equation A7 is evaluated in the same manner. In practice, if Λ is chosen appropriately, the real space summation can be neglected entirely without any appreciable loss in fidelity; and we used this simplification in the present study with $\Lambda = 0.2$ Å^{-1}.

While the strain dependence of all variables has been suppressed throughout this appendix, the evaluation of

the strain derivatives of the dynamical matrix (see Eq. A4) may be required. Here we present the strain derivatives of the reciprocal lattice points and basis atom positions, and neglect the strain dependence of the dielectric tensor and the Born effective charges, as both are small effects. The strain derivative of the reciprocal space lattice vectors with respect to a Biot strain component in the absence of rotation is given by

$$\frac{\partial \mathbf{Q}(\boldsymbol{\epsilon})}{\partial \epsilon_i} = -\mathbf{Q}(\boldsymbol{\epsilon})\hat{\boldsymbol{\lambda}}_i((\hat{\mathbf{1}} + \hat{\boldsymbol{\epsilon}})^{-1})^{\mathsf{T}}, \qquad \text{(A15)}$$

It should be noted that Eq. A15 recovers the derivatives given previously for an unstrained state [90, 91]. The basis atom positions can be encoded in Cartesian coordinates $\mathbf{A}_k(\boldsymbol{\epsilon})$ or lattice coordinates $\boldsymbol{\alpha}_\kappa(\boldsymbol{\epsilon})$, where $\mathbf{A}_k(\boldsymbol{\epsilon}) = \boldsymbol{\alpha}_k(\boldsymbol{\epsilon})\hat{\mathbf{a}}(\boldsymbol{\epsilon})$. The derivative of basis atom positions with respect to strain is then

$$\frac{\partial \mathbf{A}_k(\boldsymbol{\epsilon})}{\partial \epsilon_i} = \frac{\partial \boldsymbol{\alpha}_k(\boldsymbol{\epsilon})}{\partial \epsilon_i}\hat{\mathbf{a}}(\boldsymbol{\epsilon}) + \boldsymbol{\alpha}_k(\boldsymbol{\epsilon})\hat{\mathbf{a}}_o\hat{\boldsymbol{\lambda}}_i, \qquad \text{(A16)}$$

where the first term vanishes for basis atoms with no degrees of freedom as dictated by the space group. Given the strain dependence of the lattice vectors and atomic positions, the strain derivatives of equation A7 can be evaluated (see Supplementary Material equations S23 and S24 for the first and second derivative of Eq. A10).

In thoria, the basis atom positions in direct coordinates have constant strain dependence for strains transforming like A_{1g} or E_g, but have a degree of freedom for strains transforming like T_{2g}. The strain dependence of the direct coordinates are only evaluated to first order as outlined and justified in Appendix B.

Appendix B: Determining $\mathbf{A}_i(\boldsymbol{\epsilon})$ and considerations for the expectation value of $u_\Gamma^{(j)}$

For a given space group, the basis atom positions may have degrees of freedom. These degrees of freedom are chosen by minimizing the Born-Oppenheimer potential at a given strain, yielding the classical values of the basis atom positions. The classical basis atom positions $\mathbf{A}_i(\boldsymbol{\epsilon})$ will be used as a reference point from which to define displacement amplitudes $\mathbf{u}$ at a given strain $\boldsymbol{\epsilon}$, and it should be emphasized that an exact evaluation of the Helmholtz free energy $F(T, \boldsymbol{\epsilon})$ will be independent of this choice of reference point. Here we formally outline this procedure of finding the classical basis atom positions $\mathbf{A}_i(\boldsymbol{\epsilon})$ as a function of strain. Recall that the basis atom positions are stored in n_a vectors $\mathbf{A}_i$ of length 3 (see Section II A). However, here it will be more convenient to construct a vector $\mathbf{X}$ of length $3n_a$, storing all positions. The BO potential energy can then be constructed as a function of the basis atom positions and the strain, denoted $\mathcal{V}_\Gamma(\mathbf{X}, \boldsymbol{\epsilon})$, and it should be emphasized that $\mathcal{V}_\Gamma$ only allows for $\mathbf{q} = 0$ displacements. For a given strain $\boldsymbol{\epsilon}$, the classical basis atom positions $\mathbf{X}^\star(\boldsymbol{\epsilon})$ are determined

by minimizing $\mathcal{V}_\Gamma$, given by

$$\mathbf{X}^\star(\boldsymbol{\epsilon}) = \underset{\mathbf{X}}{\text{argmin}}\, \mathcal{V}_\Gamma(\mathbf{X}, \boldsymbol{\epsilon}). \qquad \text{(B1)}$$

The above minimization can normally be performed by first-principles methods at a relatively small computational cost given that it only requires calculations using the primitive unit cell. The classical basis atom positions $\mathbf{X}^\star(\boldsymbol{\epsilon})$, which can be stored as $\mathbf{A}_i(\boldsymbol{\epsilon})$, are then used as the reference point from which to construct the displacement amplitudes $\{u_\mathbf{q}^{(j)}\}$.

In order to construct the strain derivative of the dipole-dipole contribution to the dynamical matrix (i.e. Eq. A5), we will need the strain derivative of $\mathbf{X}^\star(\boldsymbol{\epsilon})$. While the derivative can be constructed numerically, it is convenient to derive an analytic expression to leading order in strain[53], and here we evaluate the range of convergence in the case of thoria. We begin by considering the minimization condition, given by

$$\frac{\partial \mathcal{V}_\Gamma(\mathbf{X}, \boldsymbol{\epsilon})}{\partial \mathbf{X}} = \mathbf{0}, \qquad \text{(B2)}$$

and Taylor series expanding to first order in displacements and strains about $\boldsymbol{\epsilon} = \mathbf{0}$ and $\mathbf{X} = \mathbf{X}^\star(\mathbf{0})$, we obtain

$$\mathbf{0} = \frac{\partial^2 \mathcal{V}_\Gamma(\mathbf{X}, \boldsymbol{\epsilon})}{\partial \mathbf{X}^2}\bigg|_{\substack{\mathbf{X}=\mathbf{X}^\star(\mathbf{0}) \\ \boldsymbol{\epsilon}=\mathbf{0}}} (\mathbf{X} - \mathbf{X}^\star(\mathbf{0}))$$
$$+ \frac{\partial^2 \mathcal{V}_\Gamma(\mathbf{X}, \boldsymbol{\epsilon})}{\partial \mathbf{X}\partial \boldsymbol{\epsilon}}\bigg|_{\substack{\mathbf{X}=\mathbf{X}^\star(\mathbf{0}) \\ \boldsymbol{\epsilon}=\mathbf{0}}} \boldsymbol{\epsilon} + \dots. \qquad \text{(B3)}$$

We note the equivalence of the derivative in the first term
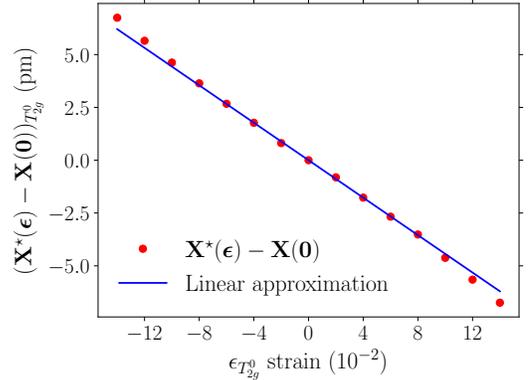
FIG. 9. The oxygen basis atom displacements projected onto the Γ-point T_{2g}^0 vector as a function of $\epsilon_{T_{2g}^0}$. The circles are the result of minimizing $\mathcal{V}_\Gamma$ at the specified value of strain, and the solid line is computed by the linear approximation (Eq. B4).

with $\hat{\mathbf{D}}_\Gamma(\mathbf{0})$ (see Eq. 63) due to the fact that $\mathbf{X} - \mathbf{X}^\star(\mathbf{0})$ are $\mathbf{q} = 0$ displacements. Solving for $\mathbf{X}^\star(\boldsymbol{\epsilon}) - \mathbf{X}^\star(\mathbf{0})$ yields

$$\mathbf{X}^\star(\boldsymbol{\epsilon}) - \mathbf{X}^\star(\mathbf{0}) = \hat{\mathbf{D}}_\Gamma(\mathbf{0})^{-1}\frac{\partial^2 \mathcal{V}_\Gamma}{\partial \mathbf{X}\partial \boldsymbol{\epsilon}}\bigg|_{\substack{\mathbf{X}=\mathbf{X}^\star(\mathbf{0}) \\ \boldsymbol{\epsilon}=\mathbf{0}}} \boldsymbol{\epsilon} + \dots \qquad \text{(B4)}$$

For the T_{2g} strains in thoria, there is a single degree of freedom in the oxygen basis atom positions, due to the fact that the space group is lowered from $Fm\bar{3}m$ to $Immm$. The only nonzero strain and displacement cross derivative in thoria is

$$\frac{\partial^2 \mathcal{V}_\Gamma(\mathbf{X}, \boldsymbol{\epsilon})}{\partial X_{T_{2g}^i} \partial \epsilon_{T_{2g}^i}}\bigg|_{\substack{\mathbf{X}=\mathbf{X}^\star(\mathbf{0})\\ \boldsymbol{\epsilon}=\mathbf{0}}}, \qquad (B5)$$

where i is any row of the T_{2g} irreducible representation. The value for Eq. B5 is 5.50, 3.76, 4.91 eV/Å for LDA, GGA, and SCAN, respectively. The resulting linear approximation to $\mathbf{X}^\star(\boldsymbol{\epsilon})$ is compared with the numerically exact result for the strain $\epsilon_{T_{2g}^0}$ (see Figure 9). The lowest order Taylor series approximation is shown to be adequate up to strains of $\epsilon_{T_{2g}^0} = 0.08$, which is within the range of strains explored by the QHA for the highest temperatures probed in our study.

Our definition of the generalized QHA, given in Eq. 62, dictates that the expectation value of the optical $\mathbf{q} = \mathbf{0}$ displacement amplitudes, present in crystals with multiple atoms per primitive unit cell, will be zero at all temperatures and strains. However, it should be emphasized that the reference point which defines the displacement amplitudes is a function of strain, given by Eq. B1. Therefore, within the generalized QHA, the average position of each atom within the unit cell is fixed at the classical $T = 0$ value at a given strain. Going

beyond the generalized QHA by adding anharmonic displacement derivatives and their strain dependence to Eq. 62 allows for changes of the average position of atoms within the unit cell as a function of temperature for a fixed strain.

Perhaps the simplest approach to go beyond the generalized QHA is to include the reference point $\mathbf{X}$ as another parameter beyond what is included in $\mathcal{V}_{qh}$, which would incorporate anharmonic contributions not encoded in the strain dependence. The reference point $\mathbf{X}$ would then serve as a set of variational parameters to be minimized over when evaluating the free energy [92], and this approach is sometimes considered a more general form of QHA[92–94]. This approach has been implemented for shear strain derivatives in crystals with the diamond cubic and zinc blende structures [94], where it is referred to as "finite temperature atomic relaxation". One can recover the same physics by taking $\mathcal{V}_{qh}$, adding all anharmonic terms associated with the $\mathbf{q} = \mathbf{0}$ displacements, and evaluating the partition function using a variational theory based on a general quadratic trial density matrix[95, 96]. Therefore, we view the finite temperature atomic relaxation approach to be a level of theory beyond the generalized QHA. Restricting the generalized QHA to mean precisely Eq. 62, where no variational parameters are used to construct the free energy, is consistent with nearly all previous QHA calculations in the literature and allows for a clear delineation between the QHA type theories and more advanced theories.

[1] E. Grneisen, Annalen der Physik **344**, 257 (1912).
[2] G. Leibfried and W. Ludwig, in *Solid State Physics*, Vol. 12, edited by F. Seitz and D. Turnbull (Academic Press, 1961) 1st ed., p. 275.
[3] P. B. Allen, Phys. Rev. B **92**, 064106 (2015).
[4] S. Baroni, P. Giannozzi, and E. Isaev, Theoretical And Computational Methods In Mineral Physics: Geophysical Applications Se Reviews In Mineralogy & Geochemistry **71**, 39 (2010).
[5] R. M. Wentzcovitch, Z. Q. Wu, and P. Carrier, Theoretical And Computational Methods In Mineral Physics: Geophysical Applications Se Reviews In Mineralogy & Geochemistry **71**, 99 (2010).
[6] P. B. Allen, Modern Physics Letters B **34**, 2050025 (2020).
[7] N. Mounet and N. Marzari, Phys. Rev. B **71**, 205214 (2005).
[8] B. B. Karki, R. M. Wentzcovitch, S. de Gironcoli, and S. Baroni, Phys. Rev. B **61**, 8793 (2000).
[9] A. Togo, L. Chaput, I. Tanaka, and G. Hug, Phys. Rev. B **81**, 174301 (2010).
[10] A. Erba, Journal Of Chemical Physics **141**, 124115 (2014).
[11] D. Dragoni, D. Ceresoli, and N. Marzari, Phys. Rev. B **91**, 104105 (2015).
[12] A. Togo and I. Tanaka, Scripta Materialia **108**, 1 (2015).
[13] L. F. Huang, X. Z. Lu, E. Tennessen, and J. M. Rondinelli, Computational Materials Science **120**, 84

(2016).
[14] M. Palumbo and A. D. corso, Journal Of Physics-condensed Matter **29**, 395401 (2017).
[15] T. J. Shao, B. Wen, R. Melnik, S. Yao, Y. Kawazoe, and Y. J. Tian, Journal Of Applied Physics **111**, 083525 (2012).
[16] C. Malica and A. D. corso, Journal Of Physics-condensed Matter **32**, 315902 (2020).
[17] R. C. Cooper, C. Lee, C. A. Marianetti, X. Wei, J. Hone, and J. W. Kysar, Phys. Rev. B **87**, 035423 (2013).
[18] X. D. Wei, B. Fragneaud, C. A. Marianetti, and J. W. Kysar, Phys. Rev. B **80**, 205407 (2009).
[19] T. F. Cao, D. Cuffari, and A. Bongiorno, Phys. Rev. Lett. **121**, 216001 (2018).
[20] H. Chen, N. A. Zarkevich, V. I. Levitas, D. D. Johnson, and X. C. Zhang, Npj Computational Materials **6**, 115 (2020).
[21] A. Hmiel, J. M. Winey, Y. M. Gupta, and M. P. Desjarlais, Phys. Rev. B **93**, 174113 (2016).
[22] G. F. Davies, Journal Of Physics And Chemistry Of Solids **35**, 1513 (1974).
[23] D. Wallace, *Thermodynamics of Crystals* (Dover, 1998).
[24] P. Carrier, R. Wentzcovitch, and J. Tsuchiya, Phys. Rev. B **76**, 064116 (2007).
[25] P. Carrier, J. F. Justo, and R. M. Wentzcovitch, Phys. Rev. B **78**, 144302 (2008).
[26] A. O. de-la Roza, D. Abbasi-Prez, and V. Luaa, Computer Physics Communications **182**, 2232 (2011).

[27] Y. Wang, J. J. Wang, H. Zhang, V. R. Manga, S. L. Shang, L.-Q. Chen, and Z.-K. Liu, Journal of Physics: Condensed Matter **22**, 225404 (2010).

[28] H. H. Pham, M. E. Williams, P. Mahaffey, M. Radovic, R. Arroyave, and T. Cagin, Phys. Rev. B **84**, 064101 (2011).

[29] D. Das and S. R. Bharadwaj, *Thoria-based nuclear fuels: thermophysical and thermodynamic properties, fabrication, reprocessing, and waste management* (Springer Science & Business Media, 2013).

[30] B. Szpunar and J. A. Szpunar, Solid State Sciences **36**, 35 (2014).

[31] B. Szpunar, J. A. Szpunar, and K. S. Sim, Journal Of Physics And Chemistry Of Solids **90**, 114 (2016).

[32] L. Malakkal, B. Szpunar, J. C. Zuniga, R. K. Siripurapu, and J. A. Szpunar, International Journal Of Computational Materials Science And Engineering **5**, 1650008 (2016).

[33] Y. Lu, Y. Yang, and P. Zhang, Journal Of Physics-condensed Matter **24**, 225801 (2012).

[34] B. T. Wang, H. L. Shi, W. D. Li, and P. Zhang, Journal Of Nuclear Materials **399**, 181 (2010).

[35] H. Nakamura and M. Machida, Journal Of Nuclear Materials **478**, 56 (2016).

[36] C. Sevik and T. Cagin, Phys. Rev. B **80**, 014108 (2009).

[37] J. B. Wachtman Jr., T. G. Scuderi, and G. W. Cleek, Journal of the American Ceramic Society **45**, 319 (1962).

[38] A. Momin, E. Mirza, and M. Mathews, Journal of Nuclear Materials **185**, 308 (1991).

[39] D. Taylor, British Ceramic Transactions and Journal **83**, 32 (1984).

[40] Y. Touloukian, R. Kirby, E. Taylor, and T. Lee, *Thermophysical Properties of Matter-the TPRC Data Series. Volume 13. Thermal Expansion-Nonmetallic Solids*, Tech. Rep. (Thermophysical and Electronic Properties Information Analysis Center, 1977).

[41] K. Clausen, W. Hayes, J. E. Macdonald, R. Osborn, P. G. Schnabel, M. T. Hutchings, and A. Magerl, Journal Of The Chemical Society-faraday Transactions Ii **83**, 1109 (1987).

[42] P. M. Macedo, W. Capps, and J. O. Wachtman Jr., Journal of the American Ceramic Society **47**, 651 (1964).

[43] X. Sha and R. E. Cohen, Phys. Rev. B **73**, 104303 (2006).

[44] E. Wasserman, L. Stixrude, and R. E. Cohen, Phys. Rev. B **53**, 8296 (1996).

[45] J. L. Alonso, A. Castro, P. Echenique, V. Polo, A. Rubio, and D. Zueco, New Journal Of Physics **12**, 083064 (2010).

[46] J. L. Alonso, A. Castro, J. Clemente-gallardo, P. Echenique, J. J. Mazo, V. Polo, A. Rubio, and D. Zueco, Journal Of Chemical Physics **137**, 22A533 (2012).

[47] G. Mazzola, A. Zen, and S. Sorella, Journal Of Chemical Physics **137**, 134112 (2012).

[48] J. L. Alonso, C. Bouthelier-madre, A. Castro, J. Clemente-gallardo, and J. A. Jover-galtier, New Journal Of Physics **23**, 063011 (2021).

[49] C. Truesdell and R. Toupin, The classical field theories, in *Principles of Classical Mechanics and Field Theory / Prinzipien der Klassischen Mechanik und Feldtheorie*, edited by S. Flügge (Springer Berlin Heidelberg, Berlin, Heidelberg, 1960) pp. 226–858.

[50] P. Neff, B. Eidel, and R. J. Martin, Archive For Rational Mechanics And Analysis **222**, 507 (2016).

[51] See Supplemental Material at [URL will be inserted by publisher] for TDBS signals, additional strain derivative equations and graphs, strain derivatives of the dipole-dipole term, comparisons to QSA results, examples of true stress and elastic constant calculations, irreducible derivative values, the functional form of the Taylor series of $\mathcal{V}$, and definitions of the $\mathbf{q}$-points and displacement basis vectors. Ref. [97] was cited.

[52] D. C. Wallace, Physical Review **162**, 776 (1967).

[53] M. Born and K. Huang, *Dynamical Theory of Crystal Lattices*, International series of monographs on physics (Clarendon Press, 1988).

[54] T. Barron and M. L. Klein, Proceedings Of The Physical Society Of London **85**, 523 (1965).

[55] J. Cornwell, *Group Theory in Physics* (Academic Press, London, 1997).

[56] L. Fu, M. Kornbluth, Z. Cheng, and C. A. Marianetti, Phys. Rev. B **100**, 014303 (2019).

[57] K. Parlinski, Z. Q. Li, and Y. Kawazoe, Phys. Rev. Lett. **81**, 3298 (1998).

[58] M. Mann, D. Thompson, K. Serivalsatit, T. M. Tritt, J. Ballato, and J. Kolis, Crystal Growth & Design **10**, 2146 (2010).

[59] C. A. Dennett, Z. Hua, A. Khanolkar, T. Yao, P. K. Morgan, T. A. Prusnick, N. Poudel, A. French, K. Gofryk, L. He, *et al.*, APL Materials **8**, 111103 (2020).

[60] G. Sheldrick, Inc.: Madison, WI (1997).

[61] M. S. Bryan, Y. W. Fu, K. Rickert, D. Turner, T. A. Prusnick, J. M. Mann, D. L. Abernathy, C. A. Marianetti, and M. E. Manley, Communications Physics **3**, 217 (2020).

[62] D. Hurley, R. Lewis, O. Wright, and O. Matsuda, Applied Physics Letters **93**, 113101 (2008).

[63] V. E. Gusev and P. Ruello, Applied Physics Reviews **5**, 031101 (2018).

[64] C. Thomsen, H. T. Grahn, H. J. Maris, and J. Tauc, Phys. Rev. B **34**, 4129 (1986).

[65] M. Khafizov, J. Pakarinen, L. He, H. Henderson, M. Manuel, A. Nelson, B. Jaques, D. Butt, and D. H. Hurley, Acta Materialia **112**, 209 (2016).

[66] Y. Wang, D. H. Hurley, Z. Hua, G. Sha, S. Raetz, V. E. Gusev, and M. Khafizov, Scripta Materialia **166**, 34 (2019).

[67] P. E. Blochl, Phys. Rev. B **50**, 17953 (1994).

[68] G. Kresse and D. Joubert, Phys. Rev. B **59**, 1758 (1999).

[69] G. Kresse and J. Hafner, Phys. Rev. B **47**, 558 (1993).

[70] G. Kresse and J. Hafner, Phys. Rev. B **49**, 14251 (1994).

[71] G. Kresse and J. Furthmuller, Computational Materials Science **6**, 15 (1996).

[72] G. Kresse and J. Furthmuller, Phys. Rev. B **54**, 11169 (1996).

[73] J. P. Perdew and A. Zunger, Phys. Rev. B **23**, 5048 (1981).

[74] J. P. Perdew, J. A. Chevary, S. H. Vosko, K. A. Jackson, M. R. Pederson, D. J. Singh, and C. Fiolhais, Phys. Rev. B **46**, 6671 (1992).

[75] J. W. Sun, A. Ruzsinszky, and J. P. Perdew, Phys. Rev. Lett. **115**, 036402 (2015).

[76] E. B. Isaacs and C. Wolverton, Physical Review Materials **2**, 063801 (2018).

[77] J. P. Perdew, K. Burke, and M. Ernzerhof, Phys. Rev. Lett. **77**, 3865 (1996).

[78] P. E. Blochl, O. Jepsen, and O. K. Andersen, Phys. Rev. B **49**, 16223 (1994).

[79] S. Baroni, S. de Gironcoli, A. DalCorso, and P. Gian-

nozzi, Rev. Mod. Phys. **73**, 515 (2001).

[80] M. Gajdos, K. Hummer, G. Kresse, J. Furthmuller, and F. Bechstedt, Phys. Rev. B **73**, 045112 (2006).

[81] X. Gonze and C. Lee, Phys. Rev. B **55**, 10355 (1997).

[82] M. Idiri, T. LeBihan, S. Heathman, and J. Rebizant, Phys. Rev. B **70**, 014113 (2004).

[83] J. Belle and R. M. Berman 10.2172/5986642 (1984).

[84] J. S. Olsen, L. Gerward, V. Kanchana, and G. Vaitheeswaran, Journal Of Alloys And Compounds **381**, 37 (2004).

[85] R. Masuki, T. Nomoto, R. Arita, and T. Tadano, Phys. Rev. B **105**, 064112 (2022).

[86] A. Tyagi and M. Mathews, Journal of nuclear materials **278**, 123 (2000).

[87] P. Giannozzi, S. de Gironcoli, P. Pavone, and S. Baroni, Phys. Rev. B **43**, 7231 (1991).

[88] Y. Wang, L. A. Zhang, S. L. Shang, Z. K. Liu, and L. Q. Chen, Phys. Rev. B **88**, 024304 (2013).

[89] K. Mizokami, A. Togo, and I. Tanaka, Phys. Rev. B **97**, 224306 (2018).

[90] D. R. Hamann, X. Wu, K. M. Rabe, and D. Vanderbilt, Phys. Rev. B **71**, 035117 (2005).

[91] O. H. Nielsen and R. M. Martin, Phys. Rev. B **32**, 3792 (1985).

[92] N. L. Allan, T. H. K. Barron, and J. A. O. Bruno, The Journal of Chemical Physics **105**, 8300 (1996).

[93] E. B. Tadmor and R. E. Miller, *Modeling materials: continuum, atomistic and multiscale techniques* (Cambridge University Press, 2011).

[94] C. Malica, *From ab-initio thermodynamics to quasi-harmonic thermoelastic properties of crystals: A new workflow and selected applications*, Ph.D. thesis, International School for Advanced Studies (2021).

[95] D. J. Hooton, Philosophical Magazine **46**, 422 (1955).

[96] R. Bianco, I. Errea, L. Paulatto, M. Calandra, and F. Mauri, Phys. Rev. B **96**, 014111 (2017).

[97] T. Sonehara, E. Tatsu, S. Saikan, and S. Ohno, Journal of Applied Physics **101**, 103507 (2007), https://doi.org/10.1063/1.2732450.